

# Lattice Green function for extended defect calculations: Computation and error estimation with long-range forces

D. R. Trinkle\*

*Materials and Manufacturing Directorate, Air Force Research Laboratory,*

*Wright Patterson Air Force Base, Dayton, Ohio 45433-7817*

(Dated: August 10, 2018)

## Abstract

Computing the atomic geometry of lattice defects—point defects, dislocations, crack tips, surfaces, or boundaries—requires an accurate coupling of the local strain field to the long-range elastic field. Periodic boundary conditions used by classical potentials or density-functional theory may not accurately reproduce the correct bulk response to an isolated defect; this is especially true for dislocations. Recently, flexible boundary conditions have been developed to produce the correct long-range strain field from a defect—effectively “embedding” a defect in a finite cell with infinite bulk response, isolating it from either periodic images or free surfaces. Flexible boundary conditions require the calculation of the bulk response with the lattice Green function (LGF). While the LGF can be computed from the dynamical matrix, for supercell methods (periodic boundary conditions) it can only be calculated up to a maximum range. We illustrate how to accurately calculate the lattice Green function and estimate the error using a cutoff dynamical matrix combined with knowledge of the long-range behavior of the lattice Green function. The effective range of deviation of the lattice Green function from the long-range elastic behavior provides an important length scale in multiscale quasi-continuum and flexible boundary-condition calculations, and measures the error introduced with periodic boundary conditions.

PACS numbers: 61.72.Bb, 61.72.Ji, 61.72.Lk, 61.72.Mm, 61.72.Nn, 62.20.-x

## I. INTRODUCTION

Lattice defects—e.g., interstitials, vacancies, dislocations, crack tips, free surfaces, interfaces, and boundaries—each play key roles in material properties,<sup>1</sup> and in order to understand defects, one must know their geometry. The far-field geometry for many defects is accurately described by anisotropic elasticity theory.<sup>2,3</sup> However, the elastic solution often diverges near the atomic-scale center of the defect, and in many cases the center is difficult to investigate with current microscopy techniques. This is especially true of dislocations, which control plasticity in metals<sup>1</sup> and can severely limit device utility in semiconductors.<sup>4</sup> Only recently has the geometry and electronic-structure of an isolated dislocation been calculated;<sup>5,6,7</sup> this despite the rapid advances in computer hardware and density-functional theory methods. Previous density-functional theory calculations were limited by the long-range strain field of a dislocation which is incommensurate with periodic boundary conditions; hence, only dislocation dipoles<sup>8,9</sup> or quadrupoles<sup>10,11</sup> had been computed. The advent of “flexible” or “Green function” boundary conditions—first conceived by Sinclair *et al.*,<sup>12</sup> later redeveloped for crack propagation<sup>13</sup> and for dislocations and dislocation kinks<sup>14</sup>—made possible the relaxation of the core geometry of an isolated dislocation. For a review of density-functional theory methods applied to dislocations, see [15]. Flexible boundary conditions accurately treat the long-range strain field away from the defect by using the harmonic ideal lattice response in the form of the lattice Green function. The lattice Green function determines the relaxed position of an atom given the force on it and its neighbors. Flexible boundary conditions have been used to model cracks,<sup>13,16</sup> dislocations and kinks in bcc metals with classical potentials,<sup>17,18</sup> cross-slip processes in fcc metals,<sup>19</sup> isolated screw dislocations in bcc metals and ordered intermetallics with density-functional theory,<sup>5,6,7</sup> and even vacancies and free surfaces;<sup>20</sup> for a review of flexible boundary condition approaches to nanomechanics of defects, see [21].

Flexible boundary conditions are limited by the accuracy of the lattice Green function. Many closed-form results are known for the lattice Green functions of cubic lattices with nearest neighbor interactions.<sup>22,23</sup> While the lattice Green function is intimately related to the elastic constants and dynamical matrix of a crystal, it has previously been computed for realistic potentials from relaxation of atom positions given an applied force.<sup>12</sup> Rao *et al.* employed a “direct displacement” technique where separate relaxation calculations in a two-dimensional slab are used to numerically evaluate the lattice Green function for short range, while switching to the known long-range behavior of the elastic Green function.<sup>14</sup> Woodward *et al.* used this same technique with

density-functional theory for Mo, Ta, and TiAl, and found the lattice Green function matched the long-range behavior at distances of only 5Å, despite long-range metallic bonding.<sup>5</sup> However, this technique is dependent on the defect geometry—a lattice Green function computed for a [110]/2 fcc screw dislocation cannot be used for the fcc edge dislocation with a threading direction of [1̄12]/2. Moreover, relying on atomic relaxation can be prone to error in density-functional methods when the applied forces become small. A more accurate and efficient approach instead relies on the dynamical matrix and elastic constants, which can be computed using standard techniques.

What follows is a general and accurate method for the computation of the lattice Green function applicable for use in density-functional theory for a variety of defect geometries. In addition, we present and test an estimate of the error in the lattice Green function due to the geometry limitations of periodic-boundary conditions with density-functional theory. Currently available methods for computing the dynamical matrix in density-functional theory effectively produce a “folded” dynamical matrix, defined in an artificial supercell—whether they rely on a finite supercell or calculated on a discrete  $k$ -point grid.<sup>24,25,26,27,28,29</sup> However, the interactions in density-functional theory have an unknown range, likely to be larger than the artificial supercell. What is required to compute the lattice Green function is (1) a computational algorithm to accurately use the limited dynamical matrix information, and (2) an estimate of the error introduced from the dynamical matrix limitation.

Section II reviews the harmonic response functions in a lattice—the dynamical matrix, and lattice Green function—and relation to continuum elasticity theory. Section III derives the general procedure for accurate numerical evaluation of the lattice Green function, with specific application for zero-, one-, and two-dimensional defects (point defects, dislocations, and boundaries, respectively). Section IV derives an error estimate for the lattice Green function using only the dynamical matrix computation from a *single* supercell and elastic constants. The error estimate is numerically tested using a simple-cubic lattice with random long-range interactions, and is shown to be accurate even with supercells far smaller than the interaction range. Finally, Section V concludes with discussion of applications to defect calculations and the inherent length-scales in quasi-continuum methods used in multiscale applications.

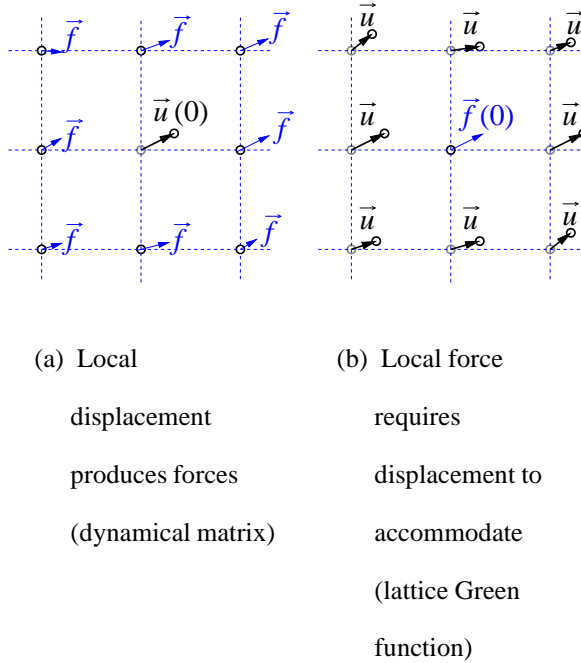


FIG. 1: Schematic of harmonic lattice response. Displacement of atoms  $\vec{u}$  in a crystal produce forces  $\vec{f}$  on neighboring atoms; the forces are given by the dynamical matrix  $\underline{D}$  for small displacements. Conversely, if an atom experiences a force, neighboring atoms must displace in order to accommodate the force; the displacement is given by the lattice Green function  $\underline{G}^L$  for small forces.

## II. HARMONIC LATTICE RESPONSE

When atoms in a crystal are subject to applied or internal forces, they respond by displacing from their ideal lattice sites; and conversely, displacement from the ideal lattice sites produces internal forces on atoms. In the case of small displacements and forces, the atoms in the lattice respond *harmonically*. Harmonic response is characterized by a linear relationship between displacement and force, given by two different lattice functions: the *dynamical matrix*, and *lattice Green function* (Figure 1 shows the responses schematically). Below we review their definitions and connections to anisotropic elasticity theory. To simplify the notation, we assume a single atom Bravais lattice; however, the approach translates readily to multiple atom Bravais lattices. Ionic crystals have additional complexities that are not addressed here.<sup>42</sup>

The dynamical matrix is well known from the classical and quantum theory of the harmonic crystal.<sup>30,31</sup> Let  $\vec{R}$  and  $\vec{R}'$  be two lattice sites in a crystal, and  $\vec{u}(\vec{R})$  and  $\vec{u}(\vec{R}')$  the displacements of

the atoms from their ideal lattice sites. Then we write the harmonic potential energy as

$$U^{\text{harm}} = \frac{1}{2} \sum_{\vec{R}\vec{R}'} \vec{u}(\vec{R}) \underline{D}(\vec{R} - \vec{R}') \vec{u}(\vec{R}'),$$

where  $\underline{D}(\vec{R} - \vec{R}')$  is a  $3 \times 3$  matrix defined at lattice sites, and the double sum ranges over all lattice sites. For small displacements, the harmonic potential energy will equal the total potential energy  $U^{\text{total}}$  of the system up to a constant if the dynamical matrix components are

$$\underline{D}_{ab}(\vec{R} - \vec{R}') = \left. \frac{\partial^2 U^{\text{total}}}{\partial u_a(\vec{R}) \partial u_b(\vec{R}')} \right|_{\vec{u}=0}.$$

In an infinite bulk lattice, there are several symmetry relations. First,  $\underline{D}$  is a function only of  $\vec{R} - \vec{R}'$ , not  $\vec{R}$  and  $\vec{R}'$  independently due to translational symmetry. Furthermore,  $\underline{D}_{ab}(\vec{R}) = \underline{D}_{ab}(-\vec{R}) = \underline{D}_{ba}(\vec{R})$  due to inversion symmetry and independence of differentiation order. Finally, if we displace every atom identically, the total energy must remain a constant; hence, the sum rule  $\sum_{\vec{R}} \underline{D}(\vec{R}) = \mathbf{0}$ . This sum rule has important consequences for the lattice Green function.

The dynamical matrix linearly relates internal displacements and forces, and connects elastic strain to elastic stress through the elastic stiffness tensor. Given displacements  $\vec{u}(\vec{R})$  at atom  $\vec{R}$ , the internal forces  $\vec{f}(\vec{R}')$  produced at atom  $\vec{R}'$  are given by

$$\vec{f}(\vec{R}') = -\frac{\partial U^{\text{harm}}}{\partial \vec{u}(\vec{R}')} = -\sum_{\vec{R}} \underline{D}(\vec{R} - \vec{R}') \vec{u}(\vec{R}). \quad (1)$$

An interesting special case of Eqn. (1) are displacements corresponding to a constant strain:  $\vec{u}(\vec{R}) = \underline{\varepsilon} \vec{R}$ , where  $\underline{\varepsilon}$  is the strain tensor. The crystal response is a constant stress tensor  $\underline{\sigma}$  which is linearly proportional to the strain by Hooke's law:  $\underline{\sigma} = \mathbf{C} \underline{\varepsilon}$ . This relationship is valid for small strains, and defines the fourth-rank elastic stiffness tensor  $\mathbf{C}$ . Eqn. (1) gives a connection between the elastic constants  $C_{abcd}$  and the dynamical matrix,

$$-\sum_{\vec{R}} \underline{D}_{ab}(\vec{R}) R_c R_d = V(C_{acbd} + C_{adbc}), \quad (2)$$

where  $V$  is the volume of the unit cell. Eqn. (2) can also be derived using the method of long-waves.<sup>30</sup> Hence, the elastic constants contain information about long-range behavior of the dynamical matrix.

The lattice Green function<sup>43</sup> linearly relates the forces on each atom to its displacement from the ideal lattice. That is,

$$\vec{u}(\vec{R}') = -\sum_{\vec{R}} \underline{G}^L(\vec{R} - \vec{R}') \vec{f}(\vec{R}), \quad (3)$$

where  $\underline{G}^L(\vec{R} - \vec{R}')$  is the lattice Green function. It obeys similar symmetries to the dynamical matrix:  $\underline{G}_{ab}^L(\vec{R}) = \underline{G}_{ab}^L(-\vec{R}) = \underline{G}_{ba}^L(\vec{R})$ . However, there is no sum rule for the lattice Green function.<sup>44</sup> At first, Eqn. (3) may not appear useful; to compute the forces in the *harmonic* potential, the displacements  $\vec{u}(\vec{R})$  must already be known. However, if instead the forces on atoms in a simulation are computed using the total energy  $U^{\text{total}}$  which is a function of relative atom positions, Eqn. (3) allows one to relax the atoms to their ideal lattice positions. In that case, the displacements are *not* known when computing the forces. In particular, the lattice Green function is used to create flexible boundary conditions<sup>12,14</sup> where an isolated defect is surrounded by atoms that respond as if they are coupled to infinite bulk. This gives an accurate treatment of the long-range stress field of a defect (such as a dislocation) while using forces from  $U^{\text{total}}$  close to the defect.

As the long-range behavior of the dynamical matrix is connected to the elastic constants, the long-range behavior of the lattice Green function is connected to the elastic Green function. The elastic Green function  $\underline{G}^E$  is a continuum function that relates a force-field  $\vec{f}(\vec{x})$  to the displacement-field  $\vec{u}(\vec{y})$ :

$$\vec{u}(\vec{y}) = - \iiint d^3x \underline{G}^E(\vec{x} - \vec{y}) \vec{f}(\vec{x}).$$

The elastic Green function can be computed knowing only the elastic response of the continuum—i.e., the elastic constant tensor  $\mathbf{C}$ .<sup>2,3</sup>  $\underline{G}^E(\vec{x})$  satisfies the partial differential equation

$$\sum_{abc} C_{iabc} \nabla_a \nabla_b \underline{G}_{cj}^E(\vec{x}) = -\delta_{ij} \delta(\vec{x}), \quad (4)$$

where  $\delta(\vec{x})$  is the Dirac delta-function. The lattice Green function must match the elastic Green function as  $\vec{R} \rightarrow \infty$ , *regardless* of how long-ranged the dynamical matrix is.

Lastly, the dynamical matrix and lattice Green function are inverses of each other. Substituting Eqn. (1) into Eqn. (3) gives

$$\sum_{\vec{R}'} \underline{G}^L(\vec{R} - \vec{R}') \underline{D}(\vec{R}') = \mathbf{1} \delta(\vec{R}), \quad (5)$$

where  $\delta(\vec{R})$  is the Kronecker delta-function. Eqn. (5) is not strictly solvable because  $\underline{D}$  is singular due to the sum rule. The singularity is due to the lack of forces from a uniform displacement of all atoms; thus, the displacements from Eqn. (3) will be known only up to a constant shift in the entire lattice. This overall translational symmetry in the lattice Green function provides for the “flexibility” in flexible boundary conditions: bulk lattice response can be simulated *without* specifying an origin for the lattice. Mathematically, the singularity in  $\underline{D}$  must be carefully treated to compute the lattice Green function accurately.

The computation of the lattice Green function is more tractable in reciprocal space. The lattice functions can be written as periodic functions of vectors  $\vec{k}$  in the Brillouin zone (BZ) of reciprocal space,<sup>31</sup>

$$\widetilde{G}^L(\vec{k}) = \sum_{\vec{R}} e^{i\vec{k}\cdot\vec{R}} \underline{G}^L(\vec{R}), \quad \underline{G}^L(\vec{R}) = V \iiint_{\text{BZ}} \frac{d^3k}{(2\pi)^3} e^{-i\vec{k}\cdot\vec{R}} \widetilde{G}^L(\vec{k}).$$

In reciprocal space, the inverse equation Eqn. (5) simplifies to  $\widetilde{G}^L(\vec{k})\widetilde{D}(\vec{k}) = \mathbf{1}$  for all  $\vec{k}$ . The singularity of  $\underline{D}$  is reduced to the gamma point  $\vec{k} = 0$ , where  $\widetilde{D}(0) = \mathbf{0}$ ; for all other points,  $\widetilde{G}^L(\vec{k}) = [\widetilde{D}(\vec{k})]^{-1}$ . The inverse is well-defined for metastable crystal structures; i.e., crystal structures without unstable phonon modes.

The computation of lattice Green function relies on accurate computation of the dynamical matrix. While computing the dynamical-matrix is straightforward for interactions with a finite cutoff, it is difficult for density-functional theory methods which may have long-range interactions (such as Friedel-oscillations). Two methods have emerged: direct force<sup>24,25,26,27</sup> and linear-response.<sup>28,29</sup> Both methods compute the reciprocal-space dynamical matrix on a discrete grid of k-points in the BZ. This is equivalent to folding the real-space dynamical matrix into an artificial supercell. We use the folded dynamical matrix to compute the lattice Green function; thus, we need to evaluate the effect of the cutoff on the accuracy of the resulting lattice Green function. We do so with the elastic constants, which can be found *separately* by computing the response of a periodic cell to uniform strains. Eqn. (2) relates the elastic constants to the long-range behavior of the true dynamical matrix. This relation provides an estimate for the deviation of the long-range elastic Green function from the lattice Green function, which in turn gives an error estimate for using the folded dynamical matrix. More importantly, this estimate does *not* rely on a convergence test computation comparing increasingly larger supercells.

Finally, it should be noted that the lattice Green function defined in Eqn. (3) can be modified for different bulk boundary conditions. Eqn. (3) defines  $\underline{G}^L$  in infinite bulk, called the 3D lattice Green function, and it is useful for computation of point defects. If the forces and displacements have periodicity along a lattice vector  $\vec{t}$ , such as in a single straight dislocation defect, the 2D lattice Green function is used:  $\sum_n \underline{G}^L(\vec{R} + n\vec{t})$ . Finally, if forces and displacements have periodicity along two lattice vectors  $\vec{t}_1$  and  $\vec{t}_2$ , such as in surfaces, grain boundaries and interfaces, the 1D lattice Green function is used:  $\sum_{mn} \underline{G}^L(\vec{R} + m\vec{t}_1 + n\vec{t}_2)$ . Despite the simple summations used to define the 2D and 1D lattice Green functions from the 3D, the sums converge conditionally. It should be remembered that the “dimensionality” of the lattice Green functions refer to the degrees

of freedom for the lattice vector  $\vec{R}$ — $\underline{G}^L$  remains a  $3 \times 3$  matrix in all cases. The dimensionality of the defect (0, 1, or 2) plus the dimensionality of the lattice Green function (3, 2, or 1) sums to 3.

### III. COMPUTATION OF LATTICE GREEN FUNCTION

The procedure for numerical computation of the lattice Green function separates the Fourier transform into pieces which can be inverse Fourier transformed accurately. The straightforward approach would be to discrete inverse Fourier transform the inverse of the dynamical matrix; however, this transform converges very slowly with increased grid spacing due to the second-order pole at the gamma point. The inversion of the dynamical matrix to compute the lattice Green function is still best performed in reciprocal space, where the large  $R$  behavior is exactly contained in the pole at  $k = 0$ . To accurately compute the lattice Green function requires an analytic treatment of the small  $k$  behavior separated from the rest of the Brillouin zone.

The separation of the lattice Green function allows the inverse Fourier transform to converge by analytically treating the second-order pole. Moreover, the separation can be evaluated for any dynamical matrix, and for any dimension. The second-order pole in  $\tilde{G}^L$  comes from the expansion of  $\tilde{D}(\vec{k})$  for small  $k$ ,

$$\begin{aligned}
\tilde{D}(\vec{k}) &= \sum_{\vec{R}} \underline{D}(\vec{R}) \exp(i\vec{k} \cdot \vec{R}) \\
&\approx \sum_{\vec{R}} \underline{D}(\vec{R}) \left[ 1 - \frac{1}{2}(\vec{k} \cdot \vec{R})^2 + \frac{1}{24}(\vec{k} \cdot \vec{R})^4 \right] \\
&= \sum_{cd} k_c k_d \left\{ -\frac{1}{2} \sum_{\vec{R}} \underline{D}(\vec{R}) R_c R_d \right\} \\
&\quad - \sum_{cdef} k_c k_d k_e k_f \left\{ -\frac{1}{24} \sum_{\vec{R}} \underline{D}(\vec{R}) R_c R_d R_e R_f \right\}.
\end{aligned} \tag{6}$$

The final expression is rewritten in terms of two functions of  $\vec{k}$  of different order in  $k$ :  $k^2 \tilde{\Lambda}^{(2)}(\hat{k}) - k^4 \tilde{\Lambda}^{(4)}(\hat{k})$ , where  $\hat{k} = \vec{k}/k$ . We relate the first function  $\tilde{\Lambda}^{(2)}(\hat{k})$  to the elastic constants by Eqn. (2),

$$\sum_{cd} k_c k_d \left\{ -\frac{1}{2} \sum_{\vec{R}} \underline{D}_{ab}(\vec{R}) R_c R_d \right\} = V \sum_{cd} k_c C_{cabd} k_d,$$

which gives  $\tilde{\Lambda}^{(2)}(\hat{k}) = V[\hat{k} \mathbf{C} \hat{k}]$ , where  $\mathbf{C}$  is the fourth-rank elastic stiffness tensor. On the other hand, the quartic function  $\tilde{\Lambda}^{(4)}(\hat{k})$  has no similar simple connection. With the definitions of  $\tilde{\Lambda}^{(2)}$

and  $\tilde{\Lambda}^{(4)}$ , the lattice Green function expands for small  $k$  as

$$\begin{aligned}
\tilde{G}^L(\vec{k}) &= [\tilde{D}(\vec{k})]^{-1} \\
&= [k^2 \tilde{\Lambda}^{(2)}(\hat{k}) - k^4 \tilde{\Lambda}^{(4)}(\hat{k}) + O(k^6)]^{-1} \\
&= k^{-2} [\tilde{\Lambda}^{(2)}(\hat{k})]^{-1} [\mathbf{1} - k^2 \tilde{\Lambda}^{(4)}(\hat{k}) [\tilde{\Lambda}^{(2)}(\hat{k})]^{-1} + O(k^4)]^{-1} \\
&= k^{-2} [\tilde{\Lambda}^{(2)}(\hat{k})]^{-1} + [\tilde{\Lambda}^{(2)}(\hat{k})]^{-1} \tilde{\Lambda}^{(4)}(\hat{k}) [\tilde{\Lambda}^{(2)}(\hat{k})]^{-1} + O(k^2) \\
&\equiv \tilde{G}^E(\vec{k}) + \tilde{G}^{dc}(\vec{k}) + O(k^2),
\end{aligned}$$

where

$$\begin{aligned}
\tilde{G}^E(\vec{k}) &\equiv k^{-2} [\tilde{\Lambda}^{(2)}(\hat{k})]^{-1} \\
&= \frac{1}{V k^2} [\hat{k} \mathbf{C} \hat{k}]^{-1},
\end{aligned} \tag{7}$$

and

$$\begin{aligned}
\tilde{G}^{dc}(\vec{k}) &\equiv [\tilde{\Lambda}^{(2)}(\hat{k})]^{-1} \tilde{\Lambda}^{(4)}(\hat{k}) [\tilde{\Lambda}^{(2)}(\hat{k})]^{-1} \\
&= \tilde{G}^E(\hat{k}) \left[ -\frac{1}{24} \sum_{\vec{R}} \underline{D}(\vec{R}) (\hat{k} \cdot \vec{R})^4 \right] \tilde{G}^E(\hat{k}).
\end{aligned} \tag{8}$$

The first function  $\tilde{G}^E$  is the second-order pole at the gamma point, which is the Fourier transform of the elastic Green function. The second function  $\tilde{G}^{dc}$  is independent of  $|k|$ , representing a discontinuity at the gamma point in the lattice Green function that appears only after the second-order pole is subtracted out; this function is called the discontinuity correction.

This expansion is used to separate the Fourier transform of the lattice Green function in the entire Brillouin zone into three pieces: the elastic Green function, discontinuity correction, and semi-continuum correction. We introduce the continuous and differentiable cutoff function  $f_{\text{cut}}(k/k_{\text{max}})$  with parameter  $0 < \alpha < 1$ ,

$$f_{\text{cut}}(x) = \begin{cases} 1 & : 0 \leq x < \alpha \\ 3(\frac{1-x}{1-\alpha})^2 - 2(\frac{1-x}{1-\alpha})^3 & : \alpha \leq x < 1 \\ 0 & : 1 \leq x \end{cases} \tag{9}$$

where  $k_{\text{max}}$  is the radius of a sphere inscribed in the Brillouin zone. While final evaluation of  $\underline{G}^L(\vec{R})$  is independent of  $\alpha$ , all computations to follow use  $\alpha = 1/2$ . Then, the semicontinuum correction is defined for  $\vec{k}$  in the first Brillouin zone as

$$\tilde{G}^{\text{sc}}(\vec{k}) = [\tilde{D}(\vec{k})]^{-1} - (\tilde{G}^E(\vec{k}) + \tilde{G}^{dc}(\vec{k})) f_{\text{cut}}(k/k_{\text{max}}). \tag{10}$$

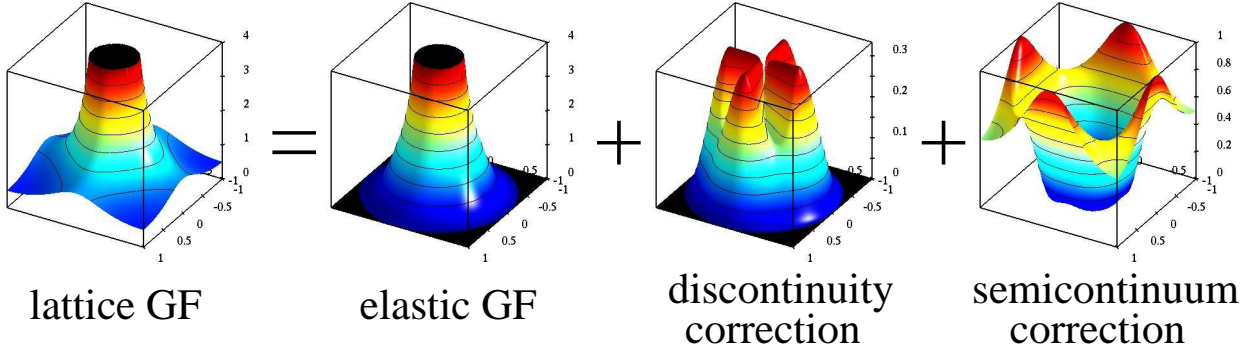


FIG. 2: Separation of lattice Green function for a square lattice in 2-dimensional reciprocal space into elastic Green function, discontinuity correction, and semicontinuum correction (note different vertical scales). The lattice Green function has the periodicity of the reciprocal lattice, and a second-order pole at the gamma point. The elastic Green function scales as  $k^{-2}$ , and is cutoff to smoothly go to zero at the Brillouin zone edges. The removal of the second-order pole creates a discontinuity independent of  $|k|$  at the gamma point; the discontinuity correction removes the discontinuity and smoothly goes to zero at the Brillouin zone edges. The remaining difference between the lattice Green function and the first two terms is the semicontinuum correction, which is smooth everywhere in the Brillouin zone.

The elimination of the second-order pole at the gamma-point by using a cutoff version of the elastic Green function is related to the semicontinuum method of Tewary.<sup>32</sup> However, his semicontinuum approach used a Gaussian cutoff which does not vanish at the Brillouin zone edge, and does not treat the discontinuity produced at the gamma point. The final lattice Green function is the sum of three pieces: elastic Green function, discontinuity correction, and semicontinuum correction.

Figure 2 shows an example of the separation of the lattice Green function into the three terms for a square lattice. The lattice Green function shown comes from a square lattice with lattice constant  $a_0 = \pi$  and nearest-neighbor interactions. For this case,  $\tilde{G}^L(k_x, k_y) = (\sin^2(\pi k_x/2) + \sin^2(\pi k_y/2))^{-1}$ . The second-order pole at origin is given by the elastic Green function  $\tilde{G}^E(k_x, k_y) = 4/(\pi|k|)^2$ ; it is multiplied by the cutoff function with  $k_{\max} = 1$  so as to vanish at the Brillouin zone edge. Subtracting the pole from the lattice Green function produces a function with a discontinuity at the gamma point. The discontinuity at the origin is given by the discontinuity correction  $\tilde{G}^{dc}(k_x, k_y) = (k_x^4 + k_y^4)/(3|k|^4)$  which is multiplied by the cutoff function. Subtracting the discontinuity produces the semicontinuum correction,  $\tilde{G}^{sc}(k_x, k_y)$ , given by Eqn. (10).

The evaluation of the lattice Green function in real space is accomplished by inverse Fourier transforming the semicontinuum correction  $\tilde{G}^{sc}$ , the cutoff elastic Green function  $\tilde{G}^E f_{\text{cut}}$ , and the

TABLE I: Overview of lattice Green function computation for different dimensionality. The dimensionality of the lattice Green function is determined by the type of defect being simulated: the defect dimensionality plus the lattice Green function dimensionality is three. While the lattice Green function has the same form in reciprocal space, the periodicity determines the range of Brillouin zone integration, and the functions used to expand the  $\hat{k}$  dependence of the elastic Green function and discontinuity correction. The range of BZ integration produces different large  $R$  behavior for both the elastic Green function—also given by elasticity theory—and the discontinuity correction. The one-dimensional case has no  $\hat{k}$  dependence, so there is no angular expansion nor is a discontinuity correction required.

	<u>3D</u>	<u>2D</u>	<u>1D</u>
Defect type: (dimensionality)	point (0D)	dislocation, crack tip (1D)	free surface, boundary (2D)
Brillouin zone integration:	full BZ	plane(s) $\perp$ to threading direction	line(s) $\perp$ to surface plane
Angular expansion in Brillouin zone:	spherical harmonics $Y_{lm}(\theta_k, \phi_k)$	Fourier series in plane $e^{in\phi_k}$	N/A
Large $R$ elastic Green function:	$R^{-1}$	$-\ln R + R^0$	$R$
Large $R$ discontinuity correction:	$R^{-3}$	$R^{-2}$	N/A

cutoff discontinuity correction  $\tilde{G}^{\text{dc}} f_{\text{cut}}$ . The semicontinuum correction  $\tilde{G}^{\text{sc}}(\vec{k})$  is evaluated on a discrete  $k$ -point grid in the Brillouin zone using Eqn. (10); inversion of the dynamical matrix for small  $k$  must be handled carefully to avoid numerical noise. A discrete inverse Fourier transform converges well with grid spacing because  $\tilde{G}^{\text{sc}}$  is smooth throughout the Brillouin zone. The cutoff elastic Green function  $\tilde{G}^{\text{E}} f_{\text{cut}}$  and discontinuity correction  $\tilde{G}^{\text{dc}} f_{\text{cut}}$  are expanded as functions of  $\hat{k}$  using spherical harmonics or a Fourier series depending on the dimensionality of the problem. In this form, their inverse Fourier transforms can be analytically reduced to a one-dimensional integral of non-singular functions over a finite range that is computed numerically to the desired accuracy. The details of this reduction depends on the periodicity of the lattice Green function. Table I gives a brief overview of the results, and Table II gives a summary of the equations.

### A. 3D lattice Green function: 0D defects

To facilitate inverse Fourier transformation, the elastic Green function  $\tilde{G}^E$  (Eqn. (7)) and discontinuity correction  $\tilde{G}^{dc}$  (Eqn. (8)) are expanded as a spherical harmonic series, whose coefficients are computed numerically. The expansions

$$\tilde{G}^E(\vec{k}) = \frac{1}{k^2} \sum_{l=0}^{L_{\max}} \sum_{m=-l}^l \tilde{G}_{lm}^E Y_{lm}(\hat{k}), \quad \tilde{G}^{dc}(\vec{k}) = \sum_{l=0}^{L_{\max}} \sum_{m=-l}^l \tilde{G}_{lm}^{dc} Y_{lm}(\hat{k}),$$

are truncated for  $l > L_{\max}$ ;  $L_{\max}$  is chosen for each expansion so that the  $lm$  components above  $L_{\max}$  are less than  $10^{-11}$  of the largest  $lm$  component below  $L_{\max}$ . Moreover, as both  $\tilde{G}^E$  and  $\tilde{G}^{dc}$  are symmetric with respect to inversion, only even  $l$  values are nonzero. The normalized spherical harmonics are given by

$$Y_{lm}(\theta, \phi) = e^{im\phi} \sqrt{\frac{2l+1}{4\pi} \frac{(l-m)!}{(l+m)!}} P_l^m(\cos \theta),$$

for  $\hat{k} = (\sin \theta \cos \phi, \sin \theta \sin \phi, \cos \theta)$ , where  $P_l^m(x)$  is the associated Legendre polynomial without the  $(-1)^m$  phase.<sup>33</sup> To compute the spherical harmonic expansion, the elastic Green function and discontinuity correction are evaluated on a spherical  $N \times N$  grid  $|\vec{k}| = 1$  given by  $\phi_i = 2\pi i/N$ , and  $\theta_j = \arccos(u_j)$ , where  $u_j$  are the  $N$  roots of the  $N^{\text{th}}$  order Legendre polynomial  $P_N(u)$ . This grid allows the computation of expansion elements up to  $L_{\max} = N/2 - 1$ . The spherical harmonic components are evaluated by (1) discrete Fourier transforming the  $\phi_i$  grid to  $m$  components, then (2) using Gaussian-Legendre quadrature with weights  $w_j$  on the  $\theta_j$  grid to produce  $l$  components:

$$\tilde{G}_{lm}^E = \frac{2\pi}{N} \sum_{j=0}^{N-1} w_j \sqrt{\frac{2l+1}{4\pi} \frac{(l-m)!}{(l+m)!}} P_l^m(u_j) \sum_{i=0}^{N-1} e^{-im\phi_i} \tilde{G}^E(\theta_j, \phi_i),$$

and identically for  $\tilde{G}^{dc}$ . As a final step, it is useful to reduce numerical error in the expansion by explicitly enforcing the point group symmetry of the lattice on the expansion; this is done using the Wigner D-matrix,<sup>34</sup> modified to take into account the effect of a symmetry operation on the  $3 \times 3$  matrix elements.

Given the spherical harmonic series, inverse Fourier transformation reduces to a single integral over a finite range. Writing the inverse Fourier transform integral in spherical harmonics over the

BZ gives

$$\begin{aligned}\underline{G}^E(\vec{R}) &= \sum_{lm}^{L_{\max}} \tilde{G}_{lm}^E \frac{V}{(2\pi)^3} \int_0^{k_{\max}} dk f_{\text{cut}}(k/k_{\max}) \iint_{4\pi} d^2\hat{k} e^{ik\hat{k}\cdot\hat{R}} Y_{lm}(\hat{k}), \\ \underline{G}^{\text{dc}}(\vec{R}) &= \sum_{lm}^{L_{\max}} \tilde{G}_{lm}^{\text{dc}} \frac{V}{(2\pi)^3} \int_0^{k_{\max}} dk k^2 f_{\text{cut}}(k/k_{\max}) \iint_{4\pi} d^2\hat{k} e^{ik\hat{k}\cdot\hat{R}} Y_{lm}(\hat{k}),\end{aligned}$$

by virtue of the cutoff function. The double integral over  $\hat{k}$  is evaluated analytically as Eqn. (A3), so

$$\begin{aligned}\underline{G}^E(\vec{R}) &= \sum_{lm}^{L_{\max}} \tilde{G}_{lm}^E Y_{lm}(\hat{R}) (-1)^{l/2} \frac{V}{2\pi^2} \int_0^{k_{\max}} dk f_{\text{cut}}(k/k_{\max}) j_l(kR), \\ \underline{G}^{\text{dc}}(\vec{R}) &= \sum_{lm}^{L_{\max}} \tilde{G}_{lm}^{\text{dc}} Y_{lm}(\hat{R}) (-1)^{l/2} \frac{V}{2\pi^2} \int_0^{k_{\max}} dk k^2 f_{\text{cut}}(k/k_{\max}) j_l(kR),\end{aligned}$$

where  $j_l(x)$  is the spherical Bessel function.

The finite one-dimensional integrals are smooth functions that can be evaluated numerically to required accuracy. For the special case of  $R = 0$ ,

$$\begin{aligned}\int_0^{k_{\max}} dk f_{\text{cut}}(k/k_{\max}) j_l(0) &= \delta_{l,0} k_{\max} \left[ 1 - \frac{1-\alpha}{2} \right], \\ \int_0^{k_{\max}} dk k^2 f_{\text{cut}}(k/k_{\max}) j_l(0) &= \delta_{l,0} k_{\max}^3 \left[ \frac{1}{3} - \frac{(1-\alpha)(2\alpha^2 + 5\alpha + 8)}{30} \right].\end{aligned}$$

For  $R \neq 0$ , we define  $f_l^{(0)}(x)$  and  $f_l^{(2)}(x)$  as

$$\begin{aligned}f_l^{(0)}(x) &\equiv \frac{2}{\pi} \int_0^x du j_l(u) f_{\text{cut}}(u/x), \\ f_l^{(2)}(x) &\equiv \frac{2}{\pi} \int_0^x du u^2 j_l(u) f_{\text{cut}}(u/x),\end{aligned}\tag{11}$$

so

$$\begin{aligned}\frac{V}{2\pi^2} \int_0^{k_{\max}} dk f_{\text{cut}}(k/k_{\max}) j_l(kR) &= \frac{V}{4\pi R} f_l^{(0)}(k_{\max}R), \\ \frac{V}{2\pi^2} \int_0^{k_{\max}} dk k^2 f_{\text{cut}}(k/k_{\max}) j_l(kR) &= \frac{V}{4\pi R^3} f_l^{(2)}(k_{\max}R).\end{aligned}$$

The  $f_l$  functions are evaluated numerically by splitting the integrals into intervals between roots of  $j_l(x)$ , and then using the QAG adaptive integration algorithm with 61 point Gauss-Kronrod rules from QUADPACK.<sup>35</sup> An important limiting case is for  $R \rightarrow \infty$  where the functions can be evaluated analytically. From Gradshteyn and Ryzhik<sup>36</sup> expression 6.561.14 gives for even  $l$

$$\lim_{x \rightarrow \infty} f_l^{(0)}(x) = \prod_{k \text{ odd}}^l k \left/ \prod_{k \text{ even}}^l k \right. ,$$

$$\lim_{x \rightarrow \infty} f_l^{(2)}(x) = (l+1)l \prod_{k \text{ odd}}^l k \left/ \prod_{k \text{ even}}^l k \right. .$$

These results are summarized in Table II.

The inverse Fourier transform of the semicontinuum correction  $\tilde{G}^{\text{sc}}$  is performed with a discrete transform on a grid in the Brillouin zone. There are different techniques for constructing a  $k$ -point mesh,<sup>37,38</sup> but a uniform grid of  $\vec{k}$ -points centered at the gamma point inside the BZ suffices. The primary requirement is that each  $k$ -point lie in the first BZ; and in that way, the points given by  $|k| < k_{\text{max}}$  form a sphere. The spacing of the grid is determined by the largest magnitude lattice vector  $R_{\text{max}}$  in the desired domain of  $\underline{G}^{\text{L}}(\vec{R})$ . To avoid aliasing errors, the grid spacing  $\Delta k$  must be smaller than  $2\pi/R_{\text{max}}$ , though a smaller spacing is preferable. For large  $R$ , substituting the elastic Green function for the lattice Green function introduces only small errors, hence reducing the effective  $R_{\text{max}}$  and  $k$ -point mesh that is used. We estimate the deviation in detail in Section IV.

## B. 2D lattice Green function: 1D defects

The introduction of a threading direction reduces the lattice Green function to a two-dimensional slab and modifies the inverse Fourier transformations. The forces and displacements of atoms around a dislocation line or a crack tip have a periodicity given by a threading lattice vector  $\vec{t}$ . The periodicity is represented in the lattice Green function by the 2D lattice Green function,  $\sum_n \underline{G}^{\text{L}}(\vec{R} + n\vec{t})$ . As with the 3D lattice Green function, evaluation of the 2D lattice Green function

is best performed in Fourier space, and inverse Fourier transforming to real space. Then,

$$\begin{aligned}
\underline{G}^{\text{L-2D}}(\vec{R}) &= \sum_{n=-\infty}^{\infty} \underline{G}^{\text{L-3D}}(\vec{R} + n\vec{t}) \\
&= \sum_{n=-\infty}^{\infty} \frac{V}{(2\pi)^3} \iiint_{\text{BZ}} d^3k e^{-i\vec{k}\cdot\vec{R}} e^{-in\vec{k}\cdot\vec{t}} \widetilde{G}^{\text{L}}(\vec{k}) \\
&= \sum_{\vec{k}_{\parallel} \in \text{BZ}} \frac{V}{|\vec{t}|} \iint_{\text{BZ}} \frac{d^2k_{\perp}}{(2\pi)^2} e^{-i(\vec{k}_{\perp} + \vec{k}_{\parallel})\cdot\vec{R}} \widetilde{G}^{\text{L}}(\vec{k}_{\perp} + \vec{k}_{\parallel})
\end{aligned} \tag{12}$$

where the (finite) summation is over  $\vec{k}_{\parallel} = 2\pi m\vec{t}/|\vec{t}|^2$  ( $m$  integer) that are inside the BZ, and two-dimensional integration is over  $\vec{k}_{\perp}$  that are perpendicular to  $\vec{t}$  and inside the BZ. This is by virtue of the summation over  $n$  which produces a delta function on  $\exp(i\vec{k} \cdot \vec{t}) - 1$ . Eqn. (12) still has a pole in  $\widetilde{G}^{\text{L}}$  to contend with, but it lies purely in the plane of  $\vec{k}_{\parallel} = \mathbf{0}$ . Hence, for  $\vec{k}_{\parallel} \neq \mathbf{0}$ , the value of  $\widetilde{G}^{\text{L}} = [\widetilde{D}]^{-1}$  is used, and a discrete inverse Fourier transform is performed. Then, the remaining difficulty is the  $1/k_{\perp}^2$  pole at the gamma point in the 2D inverse Fourier transform.

The pole at the gamma point in 2D is split into three contributions for inverse Fourier transformation: elastic Green function, discontinuity correction, semicontinuum correction. The elastic Green function  $\widetilde{G}^{\text{E}}$  and discontinuity correction  $\widetilde{G}^{\text{dc}}$  are expanded as a truncated Fourier series in the plane of  $\vec{k}_{\perp}$ ,

$$\widetilde{G}^{\text{E}}(\vec{k}_{\perp}) = \frac{1}{k_{\perp}^2} \sum_{n=0}^{N_{\text{max}}} \widetilde{G}_n^{\text{E}} e^{in\phi_k}, \quad \widetilde{G}^{\text{dc}}(\vec{k}_{\perp}) = \sum_{n=0}^{N_{\text{max}}} \widetilde{G}_n^{\text{dc}} e^{in\phi_k},$$

where  $\phi_k$  is the angle of  $\vec{k}_{\perp}$  relative to an (arbitrary) normalized in-plane reference direction  $\hat{n}_{\perp}$  ( $\hat{n}_{\perp} \cdot \vec{t} = 0$ ). The truncation  $N_{\text{max}}$  is chosen for each expansion so that the  $n$  components above  $N_{\text{max}}$  are less than  $10^{-11}$  of the largest  $n$  component below  $N_{\text{max}}$ . Since both  $\widetilde{G}^{\text{E}}$  and  $\widetilde{G}^{\text{dc}}$  have inversion symmetry, only even  $n$  values are nonzero. The Fourier series components are evaluated by computing  $\widetilde{G}^{\text{E}}(\vec{k})$  on a  $N$  element circular grid  $|\hat{k}_{\perp}| = 1$  at a series of angles  $\phi_i = 2\pi i/N$  relative to  $\hat{n}_{\perp}$ . The discrete Fourier transform gives

$$\widetilde{G}_n^{\text{E}} = \frac{1}{N} \sum_{i=0}^{N-1} e^{-in\phi_i} \widetilde{G}^{\text{E}}(\hat{k}_{\perp}(\phi_i)),$$

and identically for  $\widetilde{G}^{\text{dc}}$ . Note that  $\widetilde{G}^{\text{E}}(\vec{k})$  and  $\widetilde{G}^{\text{dc}}(\vec{k})$  are the same functions that appear in the 3D lattice Green function (given by Eqn. (7) and Eqn. (8)); for the 2D lattice Green function, they are only evaluated in the plane through the gamma point.

Given the Fourier series, inverse Fourier transformation reduces to a single integral over a finite range. The  $\vec{k}_{\parallel} \neq \mathbf{0}$  terms of Eqn. (12) have no singularities, so they can be evaluated numerically

using a discrete inverse Fourier transform with a discrete grid for  $\vec{k}_\perp$ , where construction of this grid is described below. Hence, the elastic Green function and discontinuity corrections are only evaluated for  $\vec{k}_\parallel = \mathbf{0}$ . The inverse Fourier transform integral over the BZ gives

$$\underline{G}^E(\vec{R}) [\vec{k}_\parallel = \mathbf{0}] = \sum_{n=0}^{N_{\max}} \tilde{G}_n^E \frac{V}{|\vec{t}|(2\pi)^2} \int_0^{k_{\max}} \frac{dk}{k} f_{\text{cut}}(k/k_{\max}) \int_0^{2\pi} d\phi_k e^{ikR_\perp \cos(\phi_k - \phi_R)} e^{in\phi_k},$$

where  $R_\perp = \sqrt{R^2 - (\vec{R} \cdot \vec{t})/t^2}$  is the magnitude of  $\vec{R}$  perpendicular to  $\vec{t}$ , and  $\phi_R$  is the in-plane angle of  $\vec{R}$  relative to  $\hat{n}_\perp$  ( $\phi_R = \arccos((\hat{n}_\perp \cdot \vec{R})/R_\perp)$ ). The integral over  $\phi_k$  is given by expression 8.411.1 in Gradshteyn and Ryzhik<sup>36</sup> as  $2\pi(-1)^{n/2} J_n(kR_\perp) \exp(in\phi_R)$  where  $J_n(x)$  is the Bessel function, so

$$\begin{aligned} \underline{G}^E(\vec{R}) &= \sum_{n=0}^{N_{\max}} \tilde{G}_n^E e^{in\phi_R} (-1)^{n/2} \frac{V}{|\vec{t}|2\pi} \int_0^{k_{\max}} dk k^{-1} f_{\text{cut}}(k/k_{\max}) J_n(kR_\perp), \\ \underline{G}^{\text{dc}}(\vec{R}) &= \sum_{n=0}^{N_{\max}} \tilde{G}_n^{\text{dc}} e^{in\phi_R} (-1)^{n/2} \frac{V}{|\vec{t}|2\pi} \int_0^{k_{\max}} dk k f_{\text{cut}}(k/k_{\max}) J_n(kR_\perp). \end{aligned}$$

The finite one-dimensional integrals are smooth functions for  $n > 0$  that can be evaluated numerically to required accuracy. For the special case of  $R_\perp = 0$  and  $n \neq 0$ , the integrals over  $k$  are zero. For  $n \neq 0$  and  $R_\perp \neq 0$ , we define  $F_n^{(0)}(x)$  and  $F_n^{(2)}(x)$  as

$$\begin{aligned} F_n^{(0)}(x) &\equiv \int_0^x du u^{-1} J_n(u) f_{\text{cut}}(u/x), \\ F_n^{(2)}(x) &\equiv \int_0^x du u J_n(u) f_{\text{cut}}(u/x). \end{aligned} \tag{13}$$

so

$$\begin{aligned} \frac{V}{2\pi} \int_0^{k_{\max}} dk k^{-1} f_{\text{cut}}(k/k_{\max}) J_n(kR_\perp) &= \frac{V}{2\pi} F_n^{(0)}(k_{\max}R_\perp), \\ \frac{V}{2\pi} \int_0^{k_{\max}} dk k f_{\text{cut}}(k/k_{\max}) J_n(kR_\perp) &= \frac{V}{2\pi R_\perp^2} F_n^{(2)}(k_{\max}R_\perp). \end{aligned}$$

As in the 3D case, the  $F_n$  functions for  $n \neq 0$  are evaluated numerically by splitting the integrals into intervals between roots of  $J_n(x)$ , and then using the QAG adaptive integration algorithm with 61 point Gauss-Kronrod rules from QUADPACK.<sup>35</sup> For  $u < 10^{-5}$  in the integral, using  $J_n(u)/u \approx 1/2(u/2)^{n-1}$  eliminates the division by zero. An important limiting case is for  $R_\perp \rightarrow \infty$  where

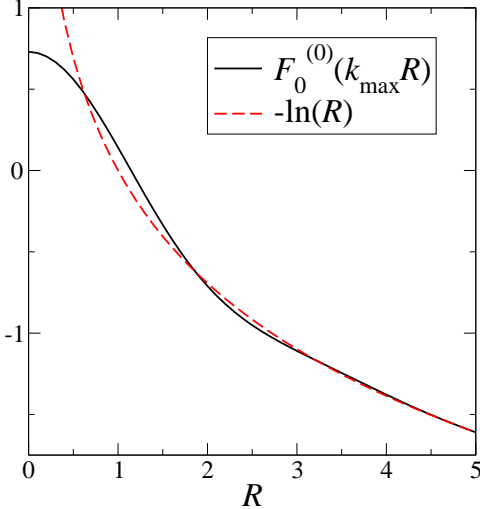


FIG. 3: Evaluation of the  $R$  scaling for the circularly symmetric portion of the 2D elastic Green function given by  $F_0^{(0)}(k_{\max}R)$ , with  $\alpha = 1/2$  and  $k_{\max} = \pi$ . The long range behavior of the elastic Green function in two dimensions scales as  $-\ln(R)$ . The cutoff function retains the correct large  $R$  behavior, with small deviations after  $R = 2$  in lattice units. Moreover, the cutoff removes the divergence at the origin.

the functions can be evaluated analytically. Expressions 6.561.14 and 6.621.4 in Gradshteyn and Ryzhik<sup>36</sup> give for  $n \neq 0$

$$\lim_{x \rightarrow \infty} F_n^{(0)}(x) = \frac{1}{n}, \quad \lim_{x \rightarrow \infty} F_n^{(2)}(x) = n.$$

The finite one-dimensional integrals for the  $n = 0$  case require additional analytic manipulation to be evaluated numerically. Figure 3 shows the convergence to the long-range behavior for  $F_0^{(0)}(k_{\max}R_{\perp})$ . The function  $F_0^{(2)}(x)$  is well-behaved for all values of  $x$ , and the limiting case of  $x \rightarrow \infty$  is 0 as given above. The  $R_{\perp} = 0, n = 0$  integral for the discontinuity correction is

$$\int_0^{k_{\max}} dk k f_{\text{cut}}(k/k_{\max}) J_0(0) = k_{\max}^2 \left[ \frac{1}{2} - \frac{(1-\alpha)(3\alpha+7)}{20} \right].$$

The  $n = 0$  integral for the elastic Green function does not converge as written, because the limit as  $R_{\perp} \rightarrow \infty$  diverges. To perform the integration, it is useful to remember from elasticity theory that the 2D elastic Green function in real space scales as  $\ln(R_{\perp})$ . The Fourier transform of  $\ln|\vec{r}|$  in two-dimensions is

$$\frac{1}{2\pi} \iint d^2r e^{i\vec{k} \cdot \vec{r}} \ln|\vec{r}| = \int_0^{\infty} dr r \ln(r) J_0(kr) = -\frac{1}{k^2},$$

which means the inverse Fourier transform integral is

$$\frac{1}{2\pi} \iint d^2k e^{-i\vec{k}\cdot\vec{r}} \frac{1}{k^2} = \int_0^\infty \frac{dk}{k} J_0(kr) = -\ln|r|.$$

Using this relation, the pole at  $k = 0$  can be evaluated analytically as

$$\begin{aligned} & \int_0^{k_{\max}} \frac{dk}{k} f_{\text{cut}}(k/k_{\max}) J_0(kR_\perp) \\ &= \int_0^\infty \frac{dk}{k} J_0(kR_\perp) + \int_{\alpha k_{\max}}^\infty \frac{dk}{k} J_0(kR_\perp) [f_{\text{cut}}(k/k_{\max}) - 1] \\ &= -\ln(R_\perp) - \int_{\alpha k_{\max}}^\infty \frac{dk}{k} J_0(kR_\perp) + \int_{\alpha k_{\max}}^{k_{\max}} \frac{dk}{k} J_0(kR_\perp) f_{\text{cut}}(k/k_{\max}) \\ &= \ln\left(\frac{\alpha k_{\max}}{2}\right) + \gamma - \frac{1}{2} \sum_{n=0}^\infty \frac{(-1)^n}{(n+1)(n+1)!^2} \left(\frac{\alpha k_{\max} R_\perp}{2}\right)^{2n+2} \\ &+ \int_{\alpha k_{\max}}^{k_{\max}} \frac{dk}{k} J_0(kR_\perp) f_{\text{cut}}(k/k_{\max}), \end{aligned}$$

where  $\gamma$  is the Euler constant ( $\gamma \approx 0.5772156649$ ). The remaining integral is evaluated numerically as before, and the series is summed numerically to within  $10^{-11}$ . The expression is finite for  $R_\perp = 0$ , and in the limit  $R_\perp \rightarrow \infty$  becomes  $-\ln(R_\perp)$  (c.f. Figure 3). The  $R_\perp = 0, n = 0$  integral for the elastic Green function is

$$\begin{aligned} & \int_0^{k_{\max}} \frac{dk}{k} f_{\text{cut}}(k/k_{\max}) J_0(0) = \ln(k_{\max}) + [\gamma - \ln 2] \\ &+ \frac{6\alpha^2(3-\alpha)\ln\alpha - (1-\alpha)(5\alpha^2 - 22\alpha + 5)}{6(1-\alpha)^3}. \end{aligned}$$

These results are summarized in Table II.

The inverse Fourier transform of the semicontinuum correction  $\tilde{G}^{\text{sc}}$  is performed with a discrete transform on a grid lying on planes in the Brillouin zone. The planes are specified by the threading direction in the lattice  $\vec{t}$ ; to form a planar grid requires two in-plane lattice vectors  $\vec{n}_\perp$  and  $\vec{m}_\perp$ . All three vectors are mutually perpendicular, though not normalized. The  $N \times M$  grid is the combination of  $\vec{k}_\parallel$  and  $\vec{k}_\perp$ , with

$$\vec{k}(t, n, m) = \frac{2\pi\vec{t}}{|\vec{t}|^2} t + \frac{2\pi\vec{n}_\perp}{|\vec{n}_\perp|^2} \frac{n}{N} + \frac{2\pi\vec{m}_\perp}{|\vec{m}_\perp|^2} \frac{m}{M},$$

where  $t, n, m$  are integers ranging over the interior of the BZ. The integers  $N$  and  $M$  specify the in-plane grid spacing, and must be chosen sufficiently large to remove aliasing effects out to  $R_{\max}$ . As for the 3D lattice Green function, the deviation between the 2D lattice Green function and 2D elastic Green function decreases with distance, thus requiring the computation of the lattice Green function out to a fixed distance dependent on required accuracy.

### C. 1D lattice Green function: 2D defects

The introduction of an infinite surface or boundary reduces the lattice Green function to a one-dimensional column and modifies the inverse Fourier transformations. The forces and displacements of atoms away from a boundary—be it a free surface, grain boundary, or interface—have a periodicity given by two non-parallel lattice vectors  $\vec{t}_1$  and  $\vec{t}_2$  lying in the boundary plane. The periodicity is represented in the lattice Green function by the 1D lattice Green function,  $\sum_{mn} \underline{G}^L(\vec{R} + m\vec{t}_1 + n\vec{t}_2)$ . As with the 3D and 2D lattice Green functions, evaluation of the 1D lattice Green function is best performed in Fourier space, and inverse Fourier transforming to real space. Then,

$$\begin{aligned} \underline{G}^{\text{L-1D}}(\vec{R}) &= \sum_{n_1, n_2=-\infty}^{\infty} \underline{G}^{\text{L-3D}}(\vec{R} + n_1\vec{t}_1 + n_2\vec{t}_2) \\ &= \sum_{n_1, n_2=-\infty}^{\infty} \frac{V}{(2\pi)^3} \iiint_{\text{BZ}} d^3 k e^{-i\vec{k}\cdot\vec{R}} e^{-in_1\vec{k}\cdot\vec{t}_1 - in_2\vec{k}\cdot\vec{t}_2} \widetilde{G}^L(\vec{k}) \\ &= \sum_{\vec{k}_{\text{plane}} \in \text{BZ}} \frac{V}{|\vec{t}_1 \times \vec{t}_2|} \int_{\text{BZ}} \frac{dk_{\perp}}{2\pi} e^{-i(\vec{k}_{\perp} + \vec{k}_{\text{plane}}) \cdot \vec{R}} \widetilde{G}^L(\vec{k}_{\perp} + \vec{k}_{\text{plane}}) \end{aligned} \quad (14)$$

where the (finite) summation is over

$$\vec{k}_{\text{plane}} = 2\pi \frac{(m_1\vec{t}_1 + m_2\vec{t}_2) \times (\vec{t}_1 \times \vec{t}_2)}{|\vec{t}_1 \times \vec{t}_2|^2},$$

( $m_1$  and  $m_2$  integer) that are inside the BZ, and one-dimensional integration is over  $\vec{k}_{\perp}$  that are parallel to  $\vec{t}_1 \times \vec{t}_2$  and inside the BZ. This is by virtue of the summation over  $n_1$  and  $n_2$ , similar to the 2D lattice Green function. Eqn. (14) still has a pole in  $\widetilde{G}^L$  to contend with, but it lies purely on the line where  $\vec{k}_{\text{plane}} = \mathbf{0}$ . Hence, for  $\vec{k}_{\text{plane}} \neq \mathbf{0}$ , the value of  $\widetilde{G}^L = [\widetilde{D}]^{-1}$  is used, and a discrete inverse Fourier transform is performed. Then, the remaining difficulty is the  $1/k_{\perp}^2$  pole at the gamma point in the 1D inverse Fourier transform.

The pole at the gamma point in 1D can be split into two contributions for inverse Fourier transformation: elastic Green function and the semicontinuum correction. For one-dimensional variation along  $\vec{k}_\perp$ , the elastic Green function is

$$\widetilde{G}^E(\vec{k}_\perp) = \frac{1}{k_\perp^2} \widetilde{G}^E,$$

where the factor  $\widetilde{G}^E = \widetilde{\Lambda}^{(2)}(\vec{t}_1 \times \vec{t}_2 / |\vec{t}_1 \times \vec{t}_2|)$  depends on  $\vec{t}_1 \times \vec{t}_2$ , and there is no remaining discontinuity at the gamma point. Thus, the semicontinuum correction no longer vanishes at the gamma point, but instead smoothly approaches a constant value. Thus, the only piece to be treated analytically is the  $1/k_\perp^2$  pole at the origin.

The inverse Fourier transformation of the elastic Green function requires the evaluation of a single integral. The elastic Green function in real space is

$$\begin{aligned} \underline{G}^E(\vec{R}) [\vec{k}_\parallel = \mathbf{0}] &= \frac{V}{|\vec{t}_1 \times \vec{t}_2|} \int_{\text{BZ}} \frac{dk_\perp}{2\pi} e^{-i\vec{k}_\perp \cdot \vec{R}} \widetilde{G}^E(\vec{k}_\perp) f_{\text{cut}}(k/k_{\max}) \\ &= \frac{V}{|\vec{t}_1 \times \vec{t}_2|} \widetilde{G}^E \int_{-k_{\max}}^{k_{\max}} \frac{dk}{2\pi} e^{-ikR_\perp} k^{-2} f_{\text{cut}}(k/k_{\max}), \end{aligned}$$

where  $R_\perp$  is the (positive) magnitude of  $\vec{R}$  perpendicular to the plane given by  $\vec{t}_1$  and  $\vec{t}_2$ . As with the 2D elastic Green function, the pole is separated off and related to the known Fourier transform giving

$$\begin{aligned} \int_{-k_{\max}}^{k_{\max}} \frac{dk}{2\pi} e^{-ikR_\perp} k^{-2} f_{\text{cut}}(k/k_{\max}) &= \int_0^{k_{\max}} dk \frac{\cos(kR_\perp)}{\pi k^2} f_{\text{cut}}(k/k_{\max}) \\ &= \int_0^{k_{\max}} dk \frac{\cos(kR_\perp)}{\pi k^2} + \int_{ak_{\max}}^{k_{\max}} dk \frac{\cos(kR_\perp)}{\pi k^2} (f_{\text{cut}}(k/k_{\max}) - 1) \\ &= \frac{1}{\pi k_{\max}} \lim_{\delta \rightarrow 0} \int_0^1 du \frac{u^2 - \delta^2}{(u^2 + \delta^2)^2} \cos(uk_{\max}R_\perp) \\ &\quad + \int_{ak_{\max}}^{k_{\max}} dk \frac{\cos(kR_\perp)}{\pi k^2} (f_{\text{cut}}(k/k_{\max}) - 1) \\ &= -\frac{|R_\perp|}{\pi} \text{Si}(k_{\max}R_\perp) - \frac{\cos(k_{\max}R_\perp)}{\pi k_{\max}} \\ &\quad + \int_{ak_{\max}}^{k_{\max}} dk \frac{\cos(kR_\perp)}{\pi k^2} (f_{\text{cut}}(k/k_{\max}) - 1). \end{aligned}$$

where  $\text{Si}(x) \equiv \int_0^x \sin(t)/t \, dt$  is the Sine integral. The remaining integral can also be evaluated in closed form, but the expression is lengthy. Two important values are  $R_\perp = 0$  and  $R_\perp \rightarrow \infty$ , which are

$$\lim_{R_\perp \rightarrow 0} \underline{G}^E(\vec{R}) = \frac{V\widetilde{G}^E}{|\vec{t}_1 \times \vec{t}_2|} \frac{3(-1 + \alpha^2 - 2\alpha \ln \alpha)}{\pi k_{\max}(1 - \alpha)^3}$$

$$\lim_{R_\perp \rightarrow \infty} \underline{G}^E(\vec{R}) = -\frac{1}{2}|R_\perp| \frac{V\widetilde{G}^E}{|\vec{t}_1 \times \vec{t}_2|}.$$

The limiting behavior of  $\underline{G}^E \sim |R_\perp|$  from elasticity theory is recovered. These results are summarized in Table II.

The inverse Fourier transform of the semicontinuum correction  $\widetilde{G}^{\text{sc}}$  is performed with a discrete transform on a grid in lines through the Brillouin zone. The grid spacing along the line must be sufficiently small to remove aliasing effects. As with the 3D and 2D lattice Green functions, the deviation between the 1D lattice and elastic Green functions decreases with distance. Thus, the elastic Green function may be substituted at a fixed distance, and requiring the computation of the full lattice Green function for a finite set of points.

#### IV. ERROR ESTIMATION FOR LGF

Table II shows that as  $R$  becomes larger, the lattice Green function asymptotically matches the elastic Green function; this matching provides the basis for an error estimate of the lattice Green function. The elastic Green function can be computed knowing only the elastic constants; in turn, the elastic constants can be computed *even for interactions without a fixed cutoff*, such as density-functional theory. Hence, while the dynamical matrix computational may induce an artificial cutoff, the asymptotic limit of the lattice Green function is known exactly. Then an estimate of the error in the lattice Green function can be determined by estimating the deviation between the elastic Green function and lattice Green function. Surprisingly, an accurate estimate can be obtained using the elastic constants and the dynamical matrix from an artificially folded supercell, even if the dynamical matrix has non-zero elements outside the supercell. Hence, a single approximate computation of the dynamical matrix in a supercell together with the elastic constants provides an estimate of the accuracy of the supercell computation. This is shown in detail below.

TABLE II: Summary of equations for lattice Green function computation for different dimensionality. The split of the lattice Green function into three pieces is given for each, along with the angular expansion. The lattice Green function in real space, the limit of large  $R$ , and value at  $R = 0$  are also given. The cutoff function  $f_{\text{cut}}$  and parameter  $\alpha$  are defined in Eqn. (9);  $k_{\text{max}}$  is the radius of a sphere inscribed in the Brillouin zone (BZ). All  $\vec{k}$  are restricted to be inside the first BZ. The finite BZ summations are done over a grid of  $N_{\text{kpt}}$  points. The function  $\Delta(x)$  is 1 for  $x = 0$ , and 0 elsewhere. The 3D integrals  $f_l^{(0)}(x)$ ,  $f_l^{(2)}(x)$  and the 2D integrals  $F_n^{(0)}(x)$ ,  $F_n^{(2)}(x)$  are defined in Eqn. (11) and Eqn. (13), respectively. For the 2D case, the periodicity is defined by a threading lattice vector  $\vec{t}$ , and  $R_{\perp}$  is the magnitude of  $\vec{R}$  perpendicular to  $\vec{t}$ . In the 1D case, the periodicity is defined by two non-parallel lattice vectors  $\vec{t}_1$  and  $\vec{t}_2$ ;  $R_{\perp}$  is the magnitude of  $\vec{R}$  perpendicular to the plane of  $\vec{t}_1$  and  $\vec{t}_2$ .

3D:	$\bar{G}^E(\vec{k}) = \frac{1}{k^2} \sum_{l \text{ even}}^{L_{\text{max}}} \sum_{m=-l}^l \bar{G}_{lm}^E Y_{lm}(\hat{k}),$	$\bar{G}^{\text{dc}}(\vec{k}) = \sum_{l \text{ even}}^{L_{\text{max}}} \sum_{m=-l}^l \bar{G}_{lm}^{\text{dc}} Y_{lm}(\hat{k}),$	$\bar{G}^{\text{sc}}(\vec{k}) = [\bar{D}(\vec{k})]^{-1} - (\bar{G}^E(\vec{k}) + \bar{G}^{\text{dc}}(\vec{k}))f_{\text{cut}}(k/k_{\text{max}})$
	$\underline{G}^L(\vec{R}) = \frac{V}{4\pi} \sum_{lm}^{L_{\text{max}}} (-1)^{l/2} \left[ \frac{1}{R} \bar{G}_{lm}^E f_l^{(0)}(k_{\text{max}} R) + \frac{1}{R^3} \bar{G}_{lm}^{\text{dc}} f_l^{(2)}(k_{\text{max}} R) \right] Y_{lm}(\hat{R}) + \frac{1}{N_{\text{kpt}}} \sum_{\vec{k} \in \text{BZ}} e^{-i\vec{k} \cdot \vec{R}} \bar{G}^{\text{sc}}(\vec{k})$		
	$\underline{G}^L(\vec{R} \rightarrow \infty) = \frac{V}{4\pi} \sum_{lm}^{L_{\text{max}}} (-1)^{l/2} \left[ \frac{1}{R} \bar{G}_{lm}^E + \frac{l(l+1)}{R^3} \bar{G}_{lm}^{\text{dc}} \right] \left( \prod_{k \text{ odd}}^l k \prod_{k \text{ even}}^l k \right) Y_{lm}(\hat{R}) + O(R^{-5})$		
	$\underline{G}^L(\vec{R} = 0) = \bar{G}_{00}^E \frac{V k_{\text{max}}}{2\pi^2} \left[ 1 - \frac{1-\alpha}{2} \right] + \bar{G}_{00}^{\text{dc}} \frac{V k_{\text{max}}^3}{2\pi^2} \left[ \frac{1}{3} - \frac{(1-\alpha)(2\alpha^2 + 5\alpha + 8)}{30} \right] + \frac{1}{N_{\text{kpt}}} \sum_{\vec{k} \in \text{BZ}} \bar{G}^{\text{sc}}(\vec{k})$		
2D:	$\bar{G}^E(\vec{k}_{\perp}) = \frac{1}{k_{\perp}^2} \sum_{n \text{ even}}^{N_{\text{max}}} \bar{G}_n^E e^{in\phi_k},$	$\bar{G}^{\text{dc}}(\vec{k}_{\perp}) = \sum_{n \text{ even}}^{N_{\text{max}}} \bar{G}_n^{\text{dc}} e^{in\phi_k},$	$\bar{G}^{\text{sc}}(\vec{k}) = [\bar{D}(\vec{k})]^{-1} - (\bar{G}^E(\vec{k}) + \bar{G}^{\text{dc}}(\vec{k}))f_{\text{cut}}(k/k_{\text{max}})\Delta(\vec{k} \cdot \vec{t})$
	$\underline{G}^L(\vec{R}) = \frac{V}{2\pi \vec{t} } \sum_n^{N_{\text{max}}} (-1)^{n/2} \left[ \bar{G}_n^E F_n^{(0)}(k_{\text{max}} R_{\perp}) + \frac{1}{R_{\perp}^2} \bar{G}_n^{\text{dc}} F_n^{(2)}(k_{\text{max}} R_{\perp}) \right] e^{in\phi_R} + \frac{1}{N_{\text{kpt}}} \sum_{\vec{k}_{\parallel} + \vec{k}_{\perp} \in \text{BZ}} e^{-i(\vec{k}_{\parallel} + \vec{k}_{\perp}) \cdot \vec{R}} \bar{G}^{\text{sc}}(\vec{k}_{\parallel} + \vec{k}_{\perp})$		
	$\underline{G}^L(R_{\perp} \rightarrow \infty) = \frac{V}{2\pi \vec{t} } \left[ -\bar{G}_0^E \ln R_{\perp} + \sum_{n=2}^{N_{\text{max}}} (-1)^{n/2} \left( \frac{1}{n} \bar{G}_n^E + \frac{n}{R_{\perp}^2} \bar{G}_n^{\text{dc}} \right) e^{in\phi_R} \right] + O(R_{\perp}^{-4})$		
	$\underline{G}^L(R_{\perp} = 0) = \bar{G}_0^E \frac{V}{2\pi \vec{t} } \left[ \ln(k_{\text{max}}) + [\gamma - \ln 2] + \frac{6\alpha^2(3-\alpha) \ln \alpha - (1-\alpha)(5\alpha^2 - 22\alpha + 5)}{6(1-\alpha)^3} \right]$		
	$+ \bar{G}_0^{\text{dc}} \frac{V k_{\text{max}}^2}{2\pi \vec{t} } \left[ \frac{1}{2} - \frac{(1-\alpha)(3\alpha + 7)}{20} \right] + \frac{1}{N_{\text{kpt}}} \sum_{\vec{k}_{\parallel} + \vec{k}_{\perp} \in \text{BZ}} e^{-i\vec{k}_{\parallel} \cdot \vec{R}} \bar{G}^{\text{sc}}(\vec{k}_{\parallel} + \vec{k}_{\perp})$		
1D:	$\bar{G}^E(\vec{k}_{\perp}) = \frac{1}{k_{\perp}^2} \bar{G}^E, \quad \bar{G}^{\text{dc}}(\vec{k}_{\perp}) = 0, \quad \bar{G}^{\text{sc}}(\vec{k}) = [\bar{D}(\vec{k})]^{-1} - \bar{G}^E(\vec{k})f_{\text{cut}}(k/k_{\text{max}})\Delta(\vec{k} \cdot \vec{t}_1)\Delta(\vec{k} \cdot \vec{t}_2)$		
	$\underline{G}^L(\vec{R}) = \frac{V}{ \vec{t}_1 \times \vec{t}_2 } \bar{G}^E \left[ -\frac{ R_{\perp} }{\pi} \text{Si}(k_{\text{max}} R_{\perp}) - \frac{\cos(k_{\text{max}} R_{\perp})}{\pi k_{\text{max}}} + \int_{\alpha k_{\text{max}}}^{k_{\text{max}}} dk \frac{\cos(k R_{\perp})}{\pi k^2} (f_{\text{cut}}(k/k_{\text{max}}) - 1) \right] + \frac{1}{N_{\text{kpt}}} \sum_{\vec{k}_{\parallel} + \vec{k}_{\perp} \in \text{BZ}} e^{-i(\vec{k}_{\parallel} + \vec{k}_{\perp}) \cdot \vec{R}} \bar{G}^{\text{sc}}(\vec{k}_{\parallel} + \vec{k}_{\perp})$		
	$\underline{G}^L(R_{\perp} \rightarrow \infty) = -\frac{1}{2}  R_{\perp}  \frac{V \bar{G}^E}{ \vec{t}_1 \times \vec{t}_2 } + O(R_{\perp}^{-1})$		
	$\underline{G}^L(R_{\perp} = 0) = \frac{V \bar{G}^E}{ \vec{t}_1 \times \vec{t}_2 } \frac{3(-1 + \alpha^2 - 2\alpha \ln \alpha)}{\pi k_{\text{max}}(1-\alpha)^3} + \frac{1}{N_{\text{kpt}}} \sum_{\vec{k}_{\parallel} + \vec{k}_{\perp} \in \text{BZ}} e^{-i\vec{k}_{\parallel} \cdot \vec{R}} \bar{G}^{\text{sc}}(\vec{k}_{\parallel} + \vec{k}_{\perp})$		

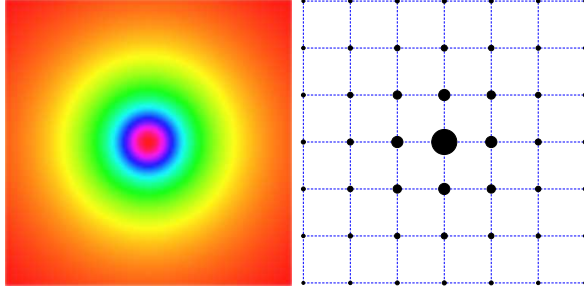


FIG. 4: Connection of solution of continuum differential equation mapped onto a lattice equation. The continuum differential equation that defines the solution on the left can be discretized by introducing a grid, and approximating derivatives with finite differences over the grid to produce a lattice equation. In the limit that the grid spacing becomes small compared to the length scale of variation of the solution, the discrete approximation matches the continuum solution. This mapping can also be reversed, by starting with a grid and a lattice equation, then taking the limit of zero grid spacing to produce a corresponding continuum differential equation.

### A. Derivation

The asymptotic connection between the lattice Green function and the elastic Green function can be understood by viewing the lattice Green function as a “numerical grid” solution to the elastic Green function differential equation, as in Figure 4. The mapping of a continuum differential equation onto a discrete grid with a lattice equation is a well known method for the numerical solution of multidimensional partial differential equations.<sup>39</sup> The (partial) derivatives can be approximated using finite differences on the grid. As the grid spacing becomes small compared to the length scale of variation of the solution, the continuum solution is recovered. Moreover, this mapping can be reversed: given a lattice equation, taking the limit of zero grid spacing can recover the continuum partial differential equation. In the case of the lattice Green function, the grid is defined by the crystalline lattice, the lattice equation by Eqn. (5) and corresponding continuum differential equation by Eqn. (4).

The analogy of the numerical solution of partial differential equations provides the basic idea for the estimation of the deviation between the lattice Green function and elastic Green function. In finite difference applications, an estimate of the discretization error can be determined by substituting the true continuum solution into the discrete equation, and using Taylor series to approximate the deviation.<sup>39</sup> For the lattice Green function equation, it is the elastic Green function

that is an approximation, but the methodology for error estimation is identical and provides the deviation between the lattice and elastic Green functions.

The relative deviation of the lattice Green function from the elastic Green function can be extracted using the real-space lattice Green function equation Eqn. (5). We begin by defining the relative deviation  $\underline{\varepsilon}^{\text{GF}}(\vec{R})$ , for  $R > 0$ , as

$$\underline{G}^{\text{L}}(\vec{R}) = \underline{G}^{\text{E}}(\vec{R}) \left\{ \mathbf{1} + \underline{\varepsilon}^{\text{GF}}(\vec{R}) \right\},$$

and substituting into Eqn. (5) for  $R > 0$  to get

$$\sum_{\vec{x}} \underline{G}^{\text{E}}(\vec{R} - \vec{x}) \underline{D}(\vec{x}) + \sum_{\vec{x}} \underline{G}^{\text{E}}(\vec{R} - \vec{x}) \underline{\varepsilon}^{\text{GF}}(\vec{R} - \vec{x}) \underline{D}(\vec{x}) = \mathbf{0}.$$

Note that while  $\underline{G}^{\text{L}}(\vec{R})$  is only defined at lattice sites,  $\underline{G}^{\text{E}}(\vec{R})$  and  $\underline{\varepsilon}^{\text{GF}}(\vec{R})$  are continuum functions. To simplify this expression, we introduce the zeroth and second order deviation functionals  $\Delta^{(0)}[\cdot]$  and  $\Delta^{(2)}[\cdot]$  of a continuum function  $f(\vec{R})$  around a point  $\vec{R}$ ,

$$\begin{aligned} \Delta^{(0)}[f](\vec{R}, \vec{x}) &\equiv \frac{1}{2} [f(\vec{R} + \vec{x}) + f(\vec{R} - \vec{x})] - f(\vec{R}), \\ \Delta^{(2)}[f](\vec{R}, \vec{x}) &\equiv \frac{1}{2} [f(\vec{R} + \vec{x}) + f(\vec{R} - \vec{x})] - f(\vec{R}) \\ &\quad - \frac{1}{2} \vec{x} \cdot \nabla \nabla f(\vec{R}) \cdot \vec{x}. \end{aligned}$$

These functionals describes the deviation between the second-order finite difference expansion of a function and the true value, with or without using the Taylor expansion. For small  $x$ ,  $\Delta^{(0)}[f](\vec{R}, \vec{x}) \approx \frac{1}{2} x^2 df^2/dR^2$  and  $\Delta^{(2)}[f](\vec{R}, \vec{x}) \approx \frac{1}{24} x^4 df^4/dR^4$ . Since  $\underline{D}(\vec{x}) = \underline{D}(-\vec{x})$ ,  $\Delta^{(0)}[\cdot]$  and  $\Delta^{(2)}[\cdot]$  can be used to write<sup>45</sup>

$$\begin{aligned} &\frac{1}{2} \left[ \underline{G}^{\text{E}}(\vec{R} - \vec{x}) \underline{D}(\vec{x}) + \underline{G}^{\text{E}}(\vec{R} + \vec{x}) \underline{D}(-\vec{x}) \right] \\ &= \left[ \underline{G}^{\text{E}}(\vec{R}) + \frac{1}{2} \vec{x} \cdot \nabla \nabla \underline{G}^{\text{E}}(\vec{R}) \cdot \vec{x} + \Delta^{(2)}[\underline{G}^{\text{E}}](\vec{R}, \vec{x}) \right] \underline{D}(\vec{x}), \\ &\frac{1}{2} \left[ \underline{G}^{\text{E}}(\vec{R} - \vec{x}) \underline{\varepsilon}^{\text{GF}}(\vec{R} - \vec{x}) \underline{D}(\vec{x}) + \underline{G}^{\text{E}}(\vec{R} + \vec{x}) \underline{\varepsilon}^{\text{GF}}(\vec{R} + \vec{x}) \underline{D}(-\vec{x}) \right] \\ &= \left[ \underline{G}^{\text{E}}(\vec{R}) \underline{\varepsilon}^{\text{GF}}(\vec{R}) + \Delta^{(0)}[\underline{G}^{\text{E}} \underline{\varepsilon}^{\text{GF}}](\vec{R}, \vec{x}) \right] \underline{D}(\vec{x}). \end{aligned}$$

Substituting these into the lattice Green function equation gives

$$\begin{aligned} &\underline{G}^{\text{E}}(\vec{R}) \left\{ \mathbf{1} + \underline{\varepsilon}^{\text{GF}}(\vec{R}) \right\} \sum_{\vec{x}} \underline{D}(\vec{x}) + \frac{1}{2} \sum_{\vec{x}} \left[ \vec{x} \cdot \nabla \nabla \underline{G}^{\text{E}}(\vec{R}) \cdot \vec{x} \right] \underline{D}(\vec{x}) \\ &+ \sum_{\vec{x}} \Delta^{(2)}[\underline{G}^{\text{E}}](\vec{R}, \vec{x}) \underline{D}(\vec{x}) + \sum_{\vec{x}} \Delta^{(0)}[\underline{G}^{\text{E}} \underline{\varepsilon}^{\text{GF}}](\vec{R}, \vec{x}) \underline{D}(\vec{x}) = \mathbf{0}. \end{aligned}$$

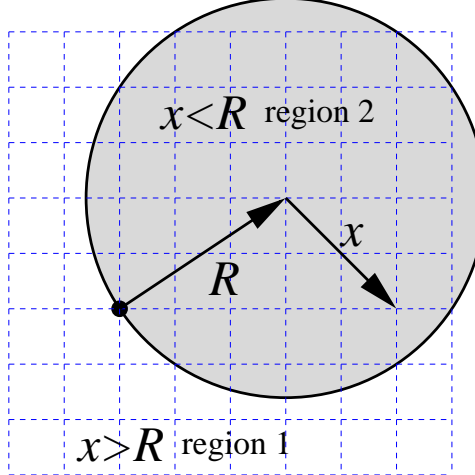


FIG. 5: Separation of error estimation summation Eqn. (15) into regions 1 and 2. The different regions can be simplified by using different approximations for  $\Delta^{(0)}[\underline{G}^E \underline{\varepsilon}^{GF}]$  and  $\Delta^{(2)}[\underline{G}^E]$ . In region 1,  $x \gg R$ , and the deviations scale as  $-\underline{G}^E(R) \underline{\varepsilon}^{GF}(R)$  and  $x^2/R^2 \underline{G}^E(R)$ , respectively. For region 2,  $x \ll R$ , and the deviations scale as  $x^2/R^2 \underline{G}^E(R) \underline{\varepsilon}^{GF}(R)$  and  $x^4/R^4 \underline{G}^E(R)$ , respectively.

The first term is zero because of the dynamical matrix sum rule. The second term is simplified to zero by using Eqn. (2),

$$\begin{aligned} & \frac{1}{2} \sum_{\vec{x}} \sum_{abc} x_a x_b \underline{D}_{cj}(\vec{x}) \nabla_a \nabla_b \underline{G}_{ic}^E(\vec{R}) \\ &= -\frac{V}{2} \sum_{abc} (C_{cajb} + C_{cbja}) \nabla_a \nabla_b \underline{G}_{ic}^E(\vec{R}) = 0, \end{aligned}$$

which is zero by virtue of Eqn. (4) and applying the interchangeability of partial derivatives, symmetries of the elastic Green function and elastic constants:  $\underline{G}_{ic}^E = \underline{G}_{ci}^E$ ,  $C_{cajb} = C_{jbca} = C_{jbac}$ ,  $C_{cbja} = C_{jabc} = C_{jabc}$ , and  $\nabla_a \nabla_b = \nabla_b \nabla_a$ . Thus,

$$\sum_{\vec{x}} \Delta^{(2)}[\underline{G}^E](\vec{R}, \vec{x}) \underline{D}(\vec{x}) + \sum_{\vec{x}} \Delta^{(0)}[\underline{G}^E \underline{\varepsilon}^{GF}](\vec{R}, \vec{x}) \underline{D}(\vec{x}) = \mathbf{0}. \quad (15)$$

To evaluate  $\underline{\varepsilon}^{GF}(\vec{R})$  in Eqn. (15) requires approximations for  $\Delta^{(0)}[\underline{G}^E \underline{\varepsilon}^{GF}]$  and  $\Delta^{(2)}[\underline{G}^E]$ . These are built by using the  $x \ll R$  and  $x \gg R$  asymptotic values over the two regions in Figure 5. For region 1 ( $x \gg R$ ), both  $\underline{G}^E \underline{\varepsilon}^{GF}(\vec{R} + \vec{x})$  and  $\underline{G}^E \underline{\varepsilon}^{GF}(\vec{R} - \vec{x})$  are much less than  $\underline{G}^E(\vec{R}) \underline{\varepsilon}^{GF}(\vec{R})$  in  $\Delta^{(0)}[\underline{G}^E \underline{\varepsilon}^{GF}](\vec{R}, \vec{x})$ . For region 2 ( $x \ll R$ ), we use the fact that  $\underline{G}^E(R) \sim 1/R$  and assume that  $\underline{\varepsilon}^{GF}(R) \sim 1/R^\beta$  for some power  $\beta$  to be determined. Using the Taylor series for small  $x$  and

choosing the maximum  $\hat{x} \cdot \hat{R} = 1$  gives the approximation in regions 1 and 2

$$\Delta^{(0)}[\underline{G}^E \underline{\varepsilon}^{GF}](\vec{R}, \vec{x}) \approx \underline{G}^E(\vec{R}) \underline{\varepsilon}^{GF}(\vec{R}) \begin{cases} -1 & : x > R \\ \frac{(\beta+1)(\beta+2)}{2} x^2 / R^2 & : x \leq R. \end{cases}$$

Similarly, for region 1 ( $x \gg R$ ),  $\Delta^{(2)}[\underline{G}^E]$  is dominated by the quadratic growth of the last term; as  $\underline{G}^E(R) \sim 1/R$ , this gives  $x^2/R^2 \underline{G}^E(R)$ . Using the next order in the Taylor series for small  $x$  in region 2 ( $x \ll R$ ), with the maximum value of  $\hat{x} \cdot \hat{R} = 1$  gives the approximation for regions 1 and 2

$$\Delta^{(2)}[\underline{G}^E](\vec{R}, \vec{x}) \approx \underline{G}^E(\vec{R}) \begin{cases} x^2/R^2 & : x > R \\ x^4/R^4 & : x \leq R. \end{cases}$$

Substituting these approximations into Eqn. (15) gives

$$\begin{aligned} & \underline{G}^E(\vec{R}) \underline{\varepsilon}^{GF}(\vec{R}) \left\{ \frac{(\beta+1)(\beta+2)}{2R^2} \sum_{|\vec{x}| \leq R} x^2 \underline{D}(\vec{x}) - \sum_{|\vec{x}| > R} \underline{D}(\vec{x}) \right\} \\ &= \underline{G}^E(\vec{R}) \left\{ \frac{1}{R^4} \sum_{|\vec{x}| \leq R} x^4 \underline{D}(\vec{x}) + \frac{1}{R^2} \sum_{|\vec{x}| > R} x^2 \underline{D}(\vec{x}) \right\}. \end{aligned}$$

The two sums over  $|\vec{x}| > R$  can be simplified by using (1) the sum rule for the dynamical matrix,

$$- \sum_{|\vec{x}| > R} \underline{D}(\vec{x}) = + \sum_{|\vec{x}| \leq R} \underline{D}(\vec{x}),$$

and (2) using the elastic constants with Eqn. (2),

$$\begin{aligned} \sum_{\vec{x} > |\vec{R}|} x^2 \underline{D}_{ab}(\vec{x}) &= \sum_{\vec{x}} x^2 \underline{D}_{ab}(\vec{x}) - \sum_{\vec{x} \leq |\vec{R}|} x^2 \underline{D}_{ab}(\vec{x}) \\ &= -2V [C_{axbx} + C_{ayby} + C_{azbz} \\ &\quad - C_{axbx}(R) - C_{ayby}(R) - C_{azbz}(R)] \\ &\equiv 2V \underline{\delta C}_{ab}(R), \end{aligned}$$

where  $C_{abcd}(R)$  refers to the elastic constants derived using Eqn. (2), summing only over lattice sites  $\vec{x} \leq R$ . We will show shortly that  $\underline{\varepsilon}^{GF}(R) \sim R^{-2}$ , so after dividing out  $\underline{G}^E(\vec{R})$  and substituting  $\beta = 2$ , we have

$$\begin{aligned} & \underline{\varepsilon}^{GF}(\vec{R}) \left\{ \frac{6}{R^2} \sum_{|\vec{x}| \leq R} x^2 \underline{D}(\vec{x}) + \sum_{|\vec{x}| \leq R} \underline{D}(\vec{x}) \right\} \\ &= \frac{1}{R^4} \sum_{|\vec{x}| \leq R} x^4 \underline{D}(\vec{x}) + \frac{2V}{R^2} \underline{\delta C}(R). \end{aligned} \tag{16}$$

Eqn. (16) can be further simplified from the small and large  $R$  limits. In the small  $R$  case (large region 1), the first terms of the left-hand and right-hand sides of Eqn. (16) become negligible. For small  $R$ , the dominant piece of  $\sum_{|\vec{x}| \leq R} \underline{D}(\vec{x})$  is  $\underline{D}(\mathbf{0})$ , so

$$\underline{\varepsilon}_{\text{region 1}}^{\text{GF}}(R) \approx \frac{2V}{R^2} \underline{\delta C}(R) [\underline{D}(\mathbf{0})]^{-1}.$$

In the large  $R$  case (large region 2), the second terms of the left-hand and right-hand side of Eqn. (16) become negligible. The summations  $\sum_{|\vec{x}| \leq R} x^2 \underline{D}(\vec{x})$  and  $\sum_{|\vec{x}| \leq R} x^4 \underline{D}(\vec{x})$  are related to the  $l = 0$  spherical harmonic expansion of  $\widetilde{G}^{\text{E}}$  and  $\widetilde{G}^{\text{dc}}$  (c.f. Appendix B and Eqn. (B1)), so

$$\underline{\varepsilon}_{\text{region 2}}^{\text{GF}}(R) \approx \frac{10}{3R^2} \frac{\widetilde{G}_{00}^{\text{dc}}(R)}{\widetilde{G}_{00}^{\text{E}}},$$

where  $\widetilde{G}_{00}^{\text{dc}}(R)$  is evaluated using the truncated dynamical matrix. Note that both pieces scale as  $R^{-2}$ , justifying the earlier choice of  $\beta = 2$ . Because the region 1 estimate falls off faster as  $R$  becomes large, and the region 2 estimate goes to zero as  $R$  goes to zero, the final approximation is to sum the two pieces

$$\underline{\varepsilon}^{\text{GF}}(R) \approx \frac{2V}{R^2} \underline{\delta C}(R) [\underline{D}(\mathbf{0})]^{-1} + \frac{10}{3R^2} \frac{\widetilde{G}_{00}^{\text{dc}}(R)}{\widetilde{G}_{00}^{\text{E}}}. \quad (17)$$

The main feature of Eqn. (17) is that the two region estimates can be determined using a *single* supercell calculation, even if the dynamical matrix lacks a finite interaction cutoff. The region 1 estimate is computed by comparing the true elastic constants to the elastic constants computed from a folded dynamical matrix, and using the supercell dimension for  $R$ . The dynamical matrix can result from a direct force computation in a finite supercell, or evaluating  $\widetilde{D}$  for a finite  $\mathbf{k}$ -point grid. In the latter case, the inverse grid spacing provides the value for  $R$ . The region 2 estimate is computable because  $\underline{G}^{\text{dc}}$  is only summed over  $\vec{x} \leq R$  for  $\underline{D}(\vec{x})$ . In both of these cases, it is assumed that the effect of folding the dynamical matrix into the supercell is approximately equivalent to truncating it outside the supercell.

## B. Numerical example of error estimate: simple-cubic lattice

While Eqn. (17) has the advantage of being computable for long-ranged dynamical matrices, it is not clear if too much accuracy has been lost in the series of approximations; so a numerical example is used to highlight the range of applicability. A series of pseudo-random long-range dynamical matrices are generated on a simple-cubic lattice with characteristics related to real

material systems; and for each, the lattice Green function, relative deviation to the elastic Green function, and region 1 and 2 estimates are computed.

The dynamical matrices are generated using  $\underline{D}(R) \sim \sin(\pi R/a_0)R^{-4}$ , cutoff at  $25a_0$ , with lattice constant  $a_0 = 1$ . The functional form is chosen to provide a long-range interaction, whose falloff is still fast enough to produce finite elastic constants in Eqn. (2). The  $\sin(\pi R/a_0)$  functional form produces a Friedel-like oscillation, as might be expected in a metallic system. The dynamical matrix elements at each site are pseudo-random numbers from a Gaussian distribution with mean 0 and standard deviation  $\sin(\pi R/a_0)R^{-4}$ . The dynamical matrix is symmetrized using the cubic point group. The elastic constants and phonons are computed; if there are unstable phonons, or the elastic anisotropy is greater than 3, the dynamical matrix is rejected. 100 random, stable, long-range simple-cubic dynamical matrices are generated in this manner; for each, the lattice and elastic Green functions along with the relative deviation are generated. The dynamical matrix is “folded down” into supercells from  $2 \times 2 \times 2$  to  $20 \times 20 \times 20$  to compute the region 1 and 2 estimates in Eqn. (17).

Figure 6 shows the true deviation and estimates from our test case for both a single example, and the average results from the 100 dynamical matrices. As expected from the derivation, the region 1 estimate dominates for small  $R$ , and falls off as the supercell becomes large enough to accurately produce the elastic constants. The region 2 estimate becomes important for large  $R$ , capturing the long-range effect from the discontinuity correction. What is especially encouraging is that the error estimate is accurate even for small supercells—such as  $2 \times 2 \times 2$ —where the supercell dynamical matrix calculation is clearly inaccurate due to the long range. This is perhaps the most impressive feature of Eqn. (17): Even when the dynamical matrix calculation comes from a small supercell, the known elastic constants can still provide an accurate error estimate *without* requiring comparisons to larger supercells. Hence, a supercell-size effect estimate on the lattice Green function computation is provided from a *single* supercell dynamical matrix computation.

## V. DISCUSSION

The deviation between the lattice Green function and elastic Green function in Eqn. (17) can be described by a single length scale  $l_{\text{elas}}$  that characterizes the recovery of continuum elastic behavior from atomistic lattice behavior:  $\underline{\varepsilon}^{\text{GF}}(R) \approx (l_{\text{elas}}/R)^2$ . This length scale determines the range out to which the lattice Green function should be computed in lieu of the elastic Green function. For

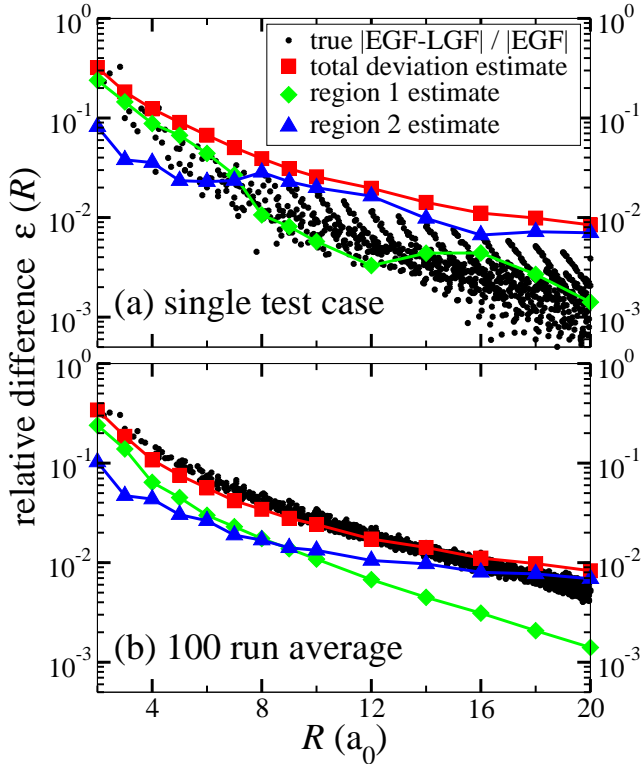


FIG. 6: Relative deviation between EGF and LGF for simple-cubic test case. The points give the deviation between the lattice Green function computed with the full dynamical matrix and the elastic Green function. The region 1 and 2 estimates are computed using the folded dynamical matrix in cubic supercells, and combined as in Eqn. (17) to produce the total deviation estimate. (a) Single random dynamical matrix shows an individual example of error estimation. (b) 100 different random dynamical matrices were computed, along with their associated LGF's. The average deviation over the ensemble average shows that we have an accurate computation of the error, even for the case of small supercells ( $2 \times 2 \times 2$ ) with the long-range dynamical matrix (cutoff at  $25a_0$ ).

example, if the magnitude of the largest lattice vector  $R_{\max}$  is greater than  $10l_{\text{elas}}$ , the lattice Green function can be computed for lattice vectors  $|\vec{R}| < 10l_{\text{elas}}$ , and the elastic Green function used for the remainder, while introducing a total error of 1%. This choice can greatly speed the computation of the lattice Green function for large simulations by (1) limiting the  $k$ -point grid size, and (2) restricting the set of points over which the full lattice Green function must be computed.

The length scale  $l_{\text{elas}}$  is also a fundamental length scale for quasi-continuum<sup>40</sup> and flexible boundary conditions methods<sup>13,14</sup> where it determines the range at which the relaxation response using elastic finite-elements or the bulk continuum is accurate compared to atomistic response.

This length is not necessarily the same as the interaction force cutoff—it may be larger or smaller. For example, the region 2 estimate of deviation for an isotropic nearest-neighbor interaction gives  $l_{\text{elas}} = \sqrt{1/6}R_{\text{nn}} \approx 0.4R_{\text{nn}}$ , which suggests transitioning from atomistic to finite-elements at twice the interaction cutoff produces errors on the order of 4% in position. On the other extreme, density-functional theory calculations in metals have shown surprisingly small  $l_{\text{elas}}$ , considering the known long-range interactions in metallic systems.<sup>5</sup> It is the small value of  $l_{\text{elas}}$  that has allowed the accurate calculation of isolated dislocations using flexible boundary condition methods in density-functional theory. Knowledge of  $l_{\text{elas}}$  is essential to constructing accurate computational cells that are large enough to produce accurate response, but do not waste computational resources treating interactions that can be replaced with elastic response.

This paper presents an accurate computational algorithm for the lattice Green function from limited dynamical matrix information together with the elastic constants. In conjunction, an accurate error estimate using the limited dynamical matrix computable from a *single* supercell computation allows measurement of the supercell-size effect. The error estimate produces a length scale  $l_{\text{elas}}$  which characterizes the crossover from atomistic harmonic response to continuum elastic response. The algorithm for lattice Green function computation together with the determination of crossover length scale has already allowed the accurate computation of single extended dislocation defects using density-functional theory.<sup>5,6,7,41</sup> The approach can also be utilized to implement flexible boundary condition methods for point defects, crack opening and tip propagation, surfaces and boundaries coupled with density-functional theory: providing chemically accurate interactions coupled with correct treatment of the long-range elastic response of extended defects.

### Acknowledgments

The author thanks R. Hennig, S. Rao, J. Wilkins, and C. Woodward for helpful discussions. This research was performed while DRT held a National Research Council Research Associateship Award at AFRL. Computational resources were provided by the Ohio Supercomputing Center.

### APPENDIX A: ANGULAR INTEGRATION IN INVERSE FOURIER TRANSFORM

The integration of the angular portion of the inverse Fourier transform in three dimensions can be performed analytically. Particular integrals referenced below can be found in Gradshteyn and

Ryzhik<sup>36</sup>.

Evaluation of the three dimensional integral

$$\iint_{4\pi} d^2 \hat{k} e^{ikR(\hat{k} \cdot \hat{R})} Y_{lm}(\hat{k}), \quad (\text{A1})$$

begins by rotating the variable of integration to a new coordinate system given by  $\hat{p}(\hat{k})$  such that  $\hat{R}$  aligned along the  $p_z$ -axis. The spherical harmonic  $Y_{lm}(\hat{k})$  is written as a linear expansion of  $Y_{lm'}(\hat{p})$

$$Y_{lm}(\hat{k}) = \sum_{m'=-l}^l a_{mm'}^{(l)}(\hat{R}) Y_{lm'}(\hat{p}), \quad (\text{A2})$$

where the  $a_{mm'}^{(l)}(\hat{R})$  coefficients will be determined later. With this expansion, Eqn. (A1) becomes

$$\sum_{m'=-l}^l a_{mm'}^{(l)}(\hat{R}) \int_0^\pi d\theta_p \sin \theta_p e^{ikR \cos \theta_p} \int_0^{2\pi} d\phi_p Y_{lm'}(\theta_p, \phi_p),$$

where  $(\theta_p, \phi_p)$  are the angular coordinates of  $\hat{p}$  with  $\vec{R}$  as the  $z$ -axis. In this coordinate system,  $\theta_p$  is the angle between  $\hat{p}$  and  $\hat{R}$ ; hence,  $\cos \theta_p = \hat{k} \cdot \hat{R}$ . The integral simplifies by (1) transforming  $u = \cos \theta_p$ , and (2) noting that the  $\phi_p$  integral is non-zero only for  $m' = 0$ . Thus, our integral reduces to

$$a_{m,0}^{(l)}(\hat{R}) \sqrt{\pi} \sqrt{2l+1} \int_{-1}^1 du P_l(u) e^{ikRu}.$$

The integral of the Legendre polynomial are expressions 7.393.1 and 7.393.2 in Gradshteyn and Ryzhik<sup>36</sup>, which has

$$\int_{-1}^1 du P_l(u) e^{ixu} = 2(i)^l j_l(x),$$

where  $j_l(x)$  is the regular spherical Bessel function,<sup>33</sup>  $\sqrt{\pi/2x} J_{l+1/2}(x)$ .

Finally,  $a_{m,0}^{(l)}(\hat{R})$  must be evaluated to produce the final expression. Eqn. (A2) can multiplied by  $Y_{ln}^*(\hat{p})$  and integrated over  $4\pi$  to give

$$\begin{aligned} a_{mn}^{(l)}(\hat{R}) &= \iint_{4\pi} d^2 \hat{p} Y_{lm}(\hat{k}(\hat{p})) Y_{ln}^*(\hat{p}) \\ &= \iint_{4\pi} d^2 \hat{k} Y_{lm}(\hat{k}) Y_{ln}^*(\hat{p}(\hat{k})). \end{aligned}$$

Then, the  $n = 0$  component is

$$a_{m,0}^{(l)}(\hat{R}) = \iint_{4\pi} d^2 \hat{k} Y_{lm}(\hat{k}) \sqrt{\frac{2l+1}{4\pi}} P_l(\cos \theta_p),$$

where  $\theta_p$  is the angle between  $\hat{p}(\hat{k})$  and the  $z$ -axis in  $p$ 's coordinate system. Given our rotation,  $\cos \theta = \hat{k} \cdot \hat{R}$ . The addition theorem for spherical harmonics,

$$P_l(\hat{k} \cdot \hat{R}) = \frac{4\pi}{2l+1} \sum_{m'=-l}^l Y_{lm'}(\hat{R}) Y_{lm'}^*(\hat{k}),$$

then gives

$$\begin{aligned} a_{m,0}^{(l)}(\hat{R}) &= \sqrt{\frac{4\pi}{2l+1}} \sum_{m'=-l}^l Y_{lm'}(\hat{R}) \iint_{4\pi} d^2\hat{k} Y_{lm}(\hat{k}) Y_{lm'}^*(\hat{k}) \\ &= \sqrt{\frac{4\pi}{2l+1}} Y_{lm}(\hat{R}). \end{aligned}$$

Combining the terms gives

$$\iint_{4\pi} d^2\hat{k} e^{ikR(\hat{k} \cdot \hat{R})} Y_{lm}(\hat{k}) = 4\pi(i)^l j_l(kR) Y_{lm}(\hat{R}). \quad (\text{A3})$$

## APPENDIX B: REGION 2 ERROR ESTIMATE

The region 2 error estimate in Eqn. (16) contains two summations over  $\vec{x}$  with  $\underline{D}(\vec{x})$  which can be approximated using the  $l = 0$  spherical harmonic components of  $\widetilde{G}^E$  and  $\widetilde{G}^{dc}$ . The quartic term  $\sum_{\vec{x}} x^4 \underline{D}(\vec{x})$  appears in the computation of  $\widetilde{G}_{00}^{dc}$ :

$$\widetilde{G}_{00}^{dc} = \frac{1}{\sqrt{4\pi}} \iint_{4\pi} d^2\hat{k} \widetilde{G}^E(\hat{k}) \left[ -\frac{1}{24} \sum_{\vec{x}} (\vec{x} \cdot \hat{k})^4 \underline{D}(\vec{x}) \right] \widetilde{G}^E(\hat{k}).$$

We can approximate  $\widetilde{G}^E(\hat{k})$  with its spherical average value,  $\widetilde{G}_{00}^E / \sqrt{4\pi}$ . The integral  $\iint_{4\pi} d^2\hat{k} (\vec{x} \cdot \hat{k})^4 = 4\pi x^4 / 5$ , so

$$\left[ -\sum_{\vec{x}} x^4 \underline{D}(\vec{x}) \right] \approx 120 \sqrt{4\pi} [\widetilde{G}_{00}^E]^{-1} \widetilde{G}_{00}^{dc} [\widetilde{G}_{00}^E]^{-1}.$$

The  $\sum_{\vec{x}} x^2 \underline{D}(\vec{x})$  term requires more egregious approximations. Starting with the definition of  $\widetilde{G}_{00}^E$ ,

$$\widetilde{G}_{00}^E = \frac{1}{\sqrt{4\pi}} \iint_{4\pi} d^2\hat{k} \left[ -\frac{1}{2} \sum_{\vec{x}} (\vec{x} \cdot \hat{k})^2 \underline{D}(\vec{x}) \right]^{-1},$$

both sides are inverted, and the inverse of the spherical average is approximated as the average of the inverse,

$$\begin{aligned} [\widetilde{G}_{00}^E]^{-1} \sqrt{4\pi} &\approx \frac{1}{4\pi} \iint_{4\pi} d^2\hat{k} \left[ -\frac{1}{2} \sum_{\vec{x}} \underline{D}(\vec{x}) (\vec{x} \cdot \hat{k})^2 \right]^{-1} \\ &= \frac{1}{4\pi} \frac{4\pi}{3} \frac{1}{2} \left[ -\sum_{\vec{x}} x^2 \underline{D}(\vec{x}) \right]. \end{aligned}$$

Inverting again gives

$$\left[ - \sum_{\vec{x}} x^2 \underline{D}(\vec{x}) \right]^{-1} \approx \frac{1}{6\sqrt{4\pi}} \widetilde{G}_{00}^E.$$

Then, for the large  $R$  limit of Eqn. (16), we have

$$\frac{1}{6R^2} \left[ - \sum_{\vec{x}} x^2 \underline{D}(\vec{x}) \right]^{-1} \left[ - \sum_{\vec{x}} x^4 \underline{D}(\vec{x}) \right] \approx \frac{10}{3R^2} \frac{\widetilde{G}_{00}^{\text{dc}}}{\widetilde{G}_{00}^E}. \quad (\text{B1})$$

The final approximation is to limit the summations to  $|\vec{x}| \leq R$ ; for that evaluation, we replace the true  $\widetilde{G}_{00}^{\text{dc}}$  with  $\widetilde{G}_{00}^{\text{dc}}(R)$ , evaluated using summations over  $|\vec{x}| \leq R$ .

Despite the approximations at use in Eqn. (B1), it is exact in an important limit: elastically isotropic crystals. Since the elastic Green function is isotropic,  $\widetilde{G}^E(\hat{k}) = \widetilde{G}_{00}^E / \sqrt{4\pi}$ , and the approximations in inverting  $\widetilde{G}_{00}^E$  are exact. Furthermore, for nearest-neighbor interactions, the left-hand side of Eqn. (B1) is exactly  $R_{\text{nn}}^2 / 6R^2$ , making  $l_{\text{elas}} = \sqrt{1/6}R_{\text{nn}}$ .

\* Department of Material Science and Engineering, University of Illinois, Urbana-Champaign, 1304 W. Green Street, Urbana, IL 61801, USA; Electronic address: dtrinkle@uiuc.edu

<sup>1</sup> P. Haasen, *Physical Metallurgy* (Cambridge University Press, 1996), Third ed., translated by J. Mordike.

<sup>2</sup> A. N. Stroh, J. Math. Phys. **41**, 77 (1962).

<sup>3</sup> D. J. Bacon, D. M. Barnett, and R. O. Scattergood, Prog. Mater. Sci. **23**, 51 (1979).

<sup>4</sup> P. Rudolph and M. Jurich, J. Crystal Growth **198/199**, 325 (1999).

<sup>5</sup> C. Woodward and S. I. Rao, Phil. Mag. A **81**, 1305 (2001).

<sup>6</sup> C. Woodward and S. Rao, Phys. Rev. Lett. **88**, 216402 (2002).

<sup>7</sup> C. Woodward and S. I. Rao, Phil. Mag. **84**, 401 (2004).

<sup>8</sup> T. A. Arias and J. D. Joannopoulos, Phys. Rev. Lett. **73**, 680 (1994).

<sup>9</sup> S. L. Frederiksen and K. W. Jacobsen, Phil. Mag. **83**, 365 (2003).

<sup>10</sup> J. R. K. Bigger, D. A. McInnes, A. P. Sutton, M. C. Payne, I. Stich, R. D. King-Smith, D. M. Bird, and L. J. Clarke, Phys. Rev. Lett. **69**, 2224 (1992).

<sup>11</sup> S. Ismail-Beigi and T. A. Arias, Phys. Rev. Lett. **84**, 1499 (2000).

<sup>12</sup> J. E. Sinclair, P. C. Gehlen, R. G. Hoagland, and J. P. Hirth, J. Appl. Phys. **49**, 3890 (1978).

<sup>13</sup> R. Thomson, S. J. Zhou, A. E. Carlsson, and V. K. Tewary, Phys. Rev. B **46**, 10613 (1992).

<sup>14</sup> S. Rao, C. Hernandez, J. P. Simmons, T. A. Parthasarathy, and C. Woodward, Phil. Mag. A **77**, 231 (1998).

<sup>15</sup> C. Woodward, Mater. Sci. Eng. A **400-401**, 59 (2005).

<sup>16</sup> L. M. Canel, A. E. Carlsson, and R. Thomson, Phys. Rev. B **52**, 158 (1995).

<sup>17</sup> S. I. Rao and C. Woodward, Phil. Mag. A **81**, 1317 (2001).

<sup>18</sup> L. H. Yang, P. Söderlind, and J. A. Moriarty, Phil. Mag. A **81**, 1355 (2001).

<sup>19</sup> S. Rao, T. A. Parthasarathy, and C. Woodward, Phil. Mag. A **79**, 1167 (1999).

<sup>20</sup> V. K. Tewary, Phys. Rev. B **69**, 094109 (2004).

<sup>21</sup> M. Ortiz and R. Phillips, Adv. Appl. Mech. **36**, 1 (1999).

<sup>22</sup> V. K. Tewary, Adv. Phys. **22**, 757 (1973).

<sup>23</sup> I. R. MacGillivray and C. A. Sholl, J. Phys. F **13**, 23 (1983).

<sup>24</sup> K. Kunc and R. M. Martin, Phys. Rev. Lett. **48**, 406 (1982).

<sup>25</sup> S. Wei and M. Y. Chou, Phys. Rev. Lett. **69**, 2799 (1992).

<sup>26</sup> W. Frank, C. Elsässer, and M. Fähnle, Phys. Rev. Lett. **74**, 1791 (1995).

<sup>27</sup> K. Parlinski, Z. Q. Li, and Y. Kawazoe, Phys. Rev. Lett. **78**, 4063 (1997).

<sup>28</sup> S. Baroni, P. Giannozzi, and A. Testa, Phys. Rev. Lett. **58**, 1861 (1987).

<sup>29</sup> A. A. Quong and B. M. Klein, Phys. Rev. B **46**, 10734 (1992).

<sup>30</sup> M. Born and K. Huang, *Dynamical Theory of Crystal Lattices* (London: Oxford University Press, 1954).

<sup>31</sup> N. W. Ashcroft and N. D. Mermin, *Solid State Physics* (Philadelphia: Saunders College, 1976).

<sup>32</sup> V. K. Tewary and R. Bullough, J. Phys. F **1**, 554 (1971).

<sup>33</sup> M. Abramowitz and I. A. Stegun, *Handbook of Mathematical Functions*, vol. 55 of *Applied Mathematics Series* (Washington: National Bureau of Standards, 1964).

<sup>34</sup> S. L. Altmann and C. J. Bradley, Phil. Trans. Royal Soc. London A **255**, 199 (1963).

<sup>35</sup> R. Piessens, E. de Doncker-Kapenga, C. Überhuber, and D. Kahaner, *QUADPACK: A subroutine package for automatic integration* (Springer-Verlag, 1983).

<sup>36</sup> I. S. Gradshteyn and I. M. Ryzhik, *Table of Integrals, Series, and Products* (Academic Press, 1994), 5th ed.

<sup>37</sup> D. J. Chadi and M. L. Cohen, Phys. Rev. B **8**, 5747 (1973).

<sup>38</sup> H. J. Monkhorst and J. D. Pack, Phys. Rev. B **13**, 5188 (1976).

<sup>39</sup> R. D. Richtmyer and K. W. Morton, *Difference Methods for Initial Value Problems* (New York: Wiley-Interscience, 1967), 2nd ed.

<sup>40</sup> R. E. Rudd and J. Q. Broughton, Phys. Rev. B **72**, 144104 (2005).

<sup>41</sup> D. R. Trinkle and C. Woodward, Science **310**, 1665 (2005).

<sup>42</sup> See [30] for a review of phonons in ionic crystals.

<sup>43</sup> This is the *static* bulk lattice Green function. The lattice Green function can be defined as a function of both time and space to model phonon propagation. In addition a defect lattice Green function can be computed using the Dyson equation. There, the starting point is the bulk lattice Green function.

<sup>44</sup> In fact, the sum of the lattice Green function over all lattice sites diverges; this requires that the sum of all forces on an infinite crystal body must vanish.

<sup>45</sup> It should be noted that the elastic Green function possess a pole at the origin; hence, the deviation functionals are technically infinite at  $\vec{x} = \pm \vec{R}$ . This complication is avoided by choosing finite values for  $\underline{G}^E$  and  $\underline{\varepsilon}^{GF}$  at the origin. This gives finite values for  $\Delta^{(0)}[\underline{G}^E \underline{\varepsilon}^{GF}](\vec{R}, \pm \vec{R})$  and  $\Delta^{(2)}[\underline{G}^E](\vec{R}, \pm \vec{R})$ . While this issue is ignored in the derivation to avoid complicating the notation further, it does not affect the results, as the elastic Green function is only evaluated at lattice sites in our derivation.